ON THE COMPUTATION AND APPLICATION OF MULTI-PERIOD SECURITY-

CONSTRAINED OPTIMAL POWER FLOW FOR REAL-TIME ELECTRICITY

MARKET OPERATIONS

A Dissertation

Presented to the Faculty of the Graduate School

of Cornell University

In Partial Fulfillment of the Requirements for the Degree of

Doctor of Philosophy

by

Hongye Wang

May 2007

ON THE COMPUTATION AND APPLICATION OF MULTI-PERIOD SECURITY-CONSTRAINED OPTIMAL POWER FLOW FOR REAL-TIME ELECTRICITY MARKET OPERATIONS

Hongye Wang, Ph. D.

Cornell University 2007

This work concerns the formulation and solution of a multi-period security-constrained optimal power flow problem for real-time electricity market operations. The solution of the proposed problem is intended to be part of the core pricing procedure for electricity trading in open markets where real energy, reactive energy, voltages support, and other system resources and services can all be traded in discrete bids and offers. Traditionally, real-time dispatching operations only involve solving single-period security-constrained optimal power flow problems. This work demonstrates the need for solving multi-period security-constrained optimal power flows. The nonsmoothness of the offer/bid-driven optimal power flow problem is studied. Three techniques, namely, a trust-region based augmented Lagrangian method, a step-controlled primal-dual interior point method, and a modified constrained cost variables method, are developed for reliable and efficient computation of large-scale nonsmooth optimal power flows. Numerical studies show that these techniques are reliable and better than some existing ones. To reduce the computational complexity, two decomposition techniques are proposed and studied. In the first one, the auxiliary problem principle method is extended to handle inequality constraints created from generator ramping limits. In the second one, binding time-coupling and contingency-coupling constraints are estimated, ranked, and filtered

before the computation is decomposed and parallelized using standard block matrix computation techniques. According to experimental results, the most promising way of solving large-scale multi-period security-constrained optimal power flow problems in real time is to combine the second decomposition method with the modified constrained cost variables method. The optimal power flow formulation and relevant computation techniques proposed in this work balance the needs for: (1) deterministic convergence, (2) accurate computation of nodal prices, (3) support of both smooth and nonsmooth costings of a variety of resources and services, such as real energy, reactive energy, voltage support, etc., (4) full active and reactive power flow modeling of large-scale systems, and (5) satisfactory worst-case performance that meets the real-time dispatching requirement.

BIOGRAPHICAL SKETCH

Hongye Wang was born in Daqing, China in 1978. He received his B.S. degree in Physics from Jilin University, Changchun, China, in 1998, and his M.S. degree in Electrical Engineering from Cornell University in 2001. From 2001 to 2004, he worked in the telecommunication industry, first as a software engineer at Nortel Networks and later as a systems engineering manager at UTStarcom Inc. From 2004 to 2007, he enrolled in the Ph.D. program in the School of Electrical and Computer Engineering at Cornell University, where he conducted research on computational issues involved in the designs and operations of electricity markets. He is a member of Sigma Xi and IEEE.

To my wife, my son, my parents, and my brother

ACKNOWLEDGMENTS

TABLE OF CONTENTS

LIST OF FIGURES

LIST OF TABLES

Chapter 1

Introduction

This work concerns the computation and application of multi-period security-constrained optimal power flow (OPF) for real-time electricity market operations. OPF has been one of the most widely studied subjects in the power system community since Carpentier first published the concept in 1962 [1]. Together with unit commitment, it forms the basis of economic planning and operation of electric power systems. With the deregulation of the power industry at its full swing, new variants of OPF have been studied and applied to market applications ranging from day-ahead market settlements to real-time pricing, from systems scheduling to generators dispatching. In its most classical mathematical representation, OPF takes in AC power balancing equations as nonlinear constraints, and minimizes the system's total operations cost based on pre-determined loads, generator capabilities, and cost curves. Transmission and voltage constraints are often integrated into this optimization problem as well, to characterize the actual power system's behaviors. Over the years, researchers have extended the OPF to include security constraints, and examined various algorithmic techniques that can speed up the computation. References [2-6] captured most of the work done in the 1970s and the 1980s, a time when several constrained optimization techniques such as the Lagrangian relaxation method, the penalty function method, and the sequential quadratic programming (SQP) method emerged as the leading nonlinear programming (NLP) methods for solving nonlinear OPF problems. The gradient method and the Newton's method were often used to

solve the underlying unconstrained optimization problems. In recent years, algorithms based on the primal-dual interior point method (PDIPM) have become popular [7-13]. To further speed up the computation of large-scale security-constrained optimal power flow (SCOPF), several decomposition and parallelization techniques have been studied [14-34].

Despite the advancements made, full-scale AC OPF's have not been widely adopted in real-time operations of large-scale power systems. Instead, system operators often use simplified OPF tools that are based on linear programming (LP) and decoupled (DC) system models [35-39]. Historically, this is mainly due to the lack of powerful computer hardware and efficient AC OPF algorithms. With the advent of fast low-cost computers, however, speed has now become a secondary concern, after algorithm robustness. The remaining prevalent argument for using LP-based DC OPF instead of NLP-based AC OPF is that LP algorithms are deterministic and always yield solutions albeit not necessarily the desired ones, while NLP algorithms are less robust and often experience convergence problems.

The emergence of electricity markets poses new challenges to the solution of OPF problems. Electricity markets are typically organized in two-settlement setups where unit commitment problems are solved in day-ahead markets, and SCOPF problems are solved every 20 minutes or so in real-time markets [36-39]. Unlike in a regulated system where the goal of computing OPF is merely minimizing the smooth quadratic cost of real-energy production, OPF computation is now part of the core pricing mechanism for electricity trading in deregulated markets where real energy, reactive energy, voltages support, and other system resources and services can all (in theory) be traded in discrete bids and offers [29, 30, 36-40]. In order to meet their legal obligations of providing timely market settlements and to ensure market fairness and efficiency, regional transmission organizations (RTO) and independent system

operators (ISO) must adopt OPF tools that provide (1) deterministic convergence, (2) accurate computation of nodal prices, (3) support of both smooth and nonsmooth costings of a variety of resources and services, such as real energy, reactive energy, voltage support, etc., (4) full active and reactive power flow modeling of large-scale systems, and (5) satisfactory worst-case performance that meets the real-time dispatching requirement. Most prior research on OPF has focused on performance issues in the context of regulated systems, without giving much emphasis to requirements (1)-(3).

This work attempts to address some of the computational challenges brought up by the deregulation. Three separate techniques, namely, a trust-region based augmented Lagrangian method (TRALM), a step-controlled primal-dual interior point method (SC-PDIPM), and a modified constrained cost variables (MCCV) method, are proposed for reliable and efficient computation of large-scale market-based OPF's. A comprehensive multi-period security-constrained OPF is formulated to replace the standalone single-period OPF that is used in today's real-time dispatching operations. In order to reduce the computational complexity of solving the comprehensive OPF problem, two decomposition techniques are proposed: one is based on the auxiliary problem principle (APP) [42], and the other is based on parallel block matrix computation and a technique that estimates and reduces binding constraints. In the former, the APP method used in [18, 19, 22, 24, 26-30] is modified to handle inequality constraints created from generator ramping limits. In the latter, the number of generator ramping constraints is reduced through a procedure that estimates, ranks, and selectively eliminates binding and non-binding constraints; the underlying matrix computation is then decomposed and parallelized at the block level without incurring much overhead of matrix fill-ins.

This chapter introduces some background information about electricity markets,

and reviews the computational techniques related to the solution of OPF problems. Chapter 2 introduces and compares several new nonsmooth optimization techniques that are tailored to the solution of market-based OPF's with piecewise costs. Chapter 3 details the two new decomposition techniques designed for solving the comprehensive multi-period security-constrained OPF problem. The work is concluded in Chapter 4.

1.1 Organization and operation of electricity markets

The electric power industry around the world has been undergoing increasingly intensive restructuring and deregulation in the past two decades [42]. In the United States, the Public Utility Regulatory Policies Act passed by the Congress in 1978 laid the groundwork for deregulation and competition by opening wholesale power markets to non-utility producers of electricity. The Congress voted to promote greater competition in the bulk power market with the passage of the Energy Policy Act of 1992. In 1996, the Federal Energy Regulatory Commission (FERC) implemented plans to allow wholesale competition in the electricity market. In the same year, FERC issued its famous Order 888, requiring utilities to open their transmission lines to competitors. Soon after, regional transmission organizations (RTO) and independent system operators (ISO) were formed in many parts of the country to administer open, competitive and nondiscriminatory wholesale markets for electricity and to ensure reliable, safe and efficient operation of major transmission systems. The established markets often utilize bid processes for electricity and transmission usage, enabling utilities and other market participants to offer electricity at competitive prices, rather than regulated rates. Today, these ISO's or RTO's typically operate two types of markets: the day-ahead markets, which schedule electricity transactions and commit power generating units at least several hours ahead the operating day, and the real-

time markets, which balance the electricity supplies and demands in real-time, provide up-to-minute spot prices, and ensure safe operation of the systems. In day-ahead scheduling operations, the unit commitment tool collects forecasted loads and market information, and solves a multi-period security-constrained optimization problem to find the cost-minimizing operation schedule for the next 24 hours. In real-time dispatching operations, the SCOPF tool takes in the operation schedule committed in the day-ahead market, receives more accurate loads information, and finds the most economical way of dispatching generators to meet the forecasted loads securely for the next 5 to 20 minutes. In both markets, locational marginal prices (LMP), which are used for final billings, are computed along with the solution of the underlying optimization problems.

1.2 Real-time market-based OPF

Although some simplified forms of OPF's have been used in real-time market operations for years now, their legitimacies have never been thoroughly evaluated. These OPF variants are often derived from the classical OPF formulation

$$
\min_{P,Q,V,\theta} \quad \sum_j C_j(P_j)
$$

$$
\begin{aligned}
\text{s.t.} \quad & FA_i(P,V,\theta) = 0 \\
& FR_i(Q,V,\theta) = 0 \\
& P_j^{\min} \leq P_j \leq P_j^{\max} \\
& Q_j^{\min} \leq Q_j \leq Q_j^{\max} \\
& V_i^{\min} \leq V_i \leq V_i^{\max} \\
& |SF_k(V,\theta)| \leq S_k^{\text{nt}-\max} \\
& |ST_k(V,\theta)| \leq S_k^{\text{nt}-\max}
\end{aligned}
\tag{1-1}
$$

$$i \in [1, NB], j \in [1, NG], k \in [1, NL] , \qquad\qquad (1\text{-}1)$$

where the objective function is the sum of all generation costs, *FA* and *FR* represent nodal balances of real and reactive power, *SF* and *ST* are branch power flows that are subject to the normal thermal limits $S^{nt\text{-}max}$, real generations *P*, reactive generations *Q*, and voltages *V* are subject to the box limits established by the operator, and *NB*, *NG*, and *NL* stand for the number of buses, the number of generators, and the number of branches, respectively. In practice, the nonlinear power balancing equations and the branch power flow constraints are often linearly approximated to reduce the computational complexity.

The simplified OPF's derived from (1-1) fail to account for several important aspects of the electricity markets, which shall be detailed in the sections below.

1.2.1 Offer/bid-driven costings of energy and non-energy resources

Unlike the energy-cost minimization role that the traditional OPF plays in the operation of a regulated power system, the objective of a market-based OPF is to minimize the total operations cost based on offers and bids placed for both energy and non-energy resources and services. Market operators may also choose to include additional cost items to model reliability and other public goods. As a result, the cost curves embedded in the objective function of the market-based OPF differ from those of the traditional OPF in three aspects:

- Shape – The cost curves derived from market offers and bids are in nonsmooth piecewise forms, while the cost curves used in the traditional OPF are often in smooth quadratic forms. Figure 1.1 illustrates the two different shapes of cost curves. Since the ability of placing fine-grain offers/bids is desirable to many market participants, market-based OPF tools must handle extremely nonsmooth objective functions. Note that cost curves in the market-based OPF
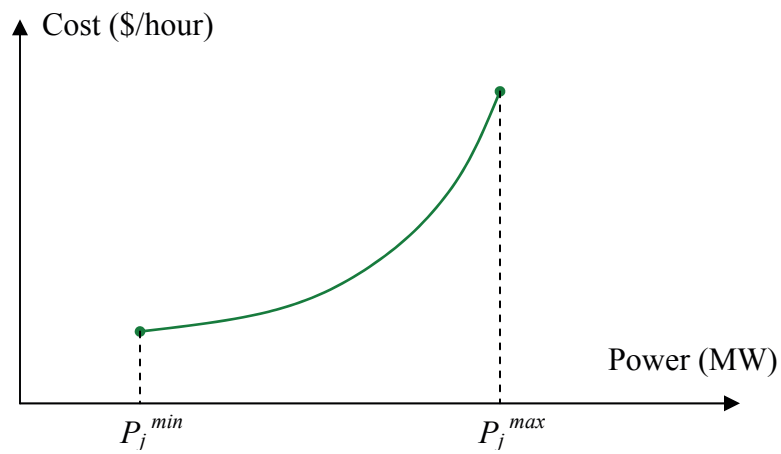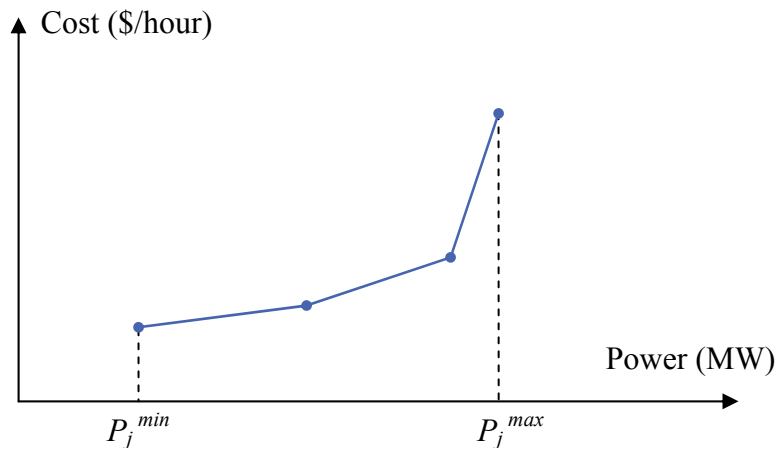
Figure 1.1 Example energy cost curves used in OPF's: (a) a quadratic energy cost curve for the traditional OPF; (b) a 3-segment piecewise linear energy cost curve for an offer/bid-driven market-based OPF.

may also take non-convex forms, which further complicates the optimization.

- Dimension – The traditional OPF only concerns energy costs, while the market-based OPF deals with both energy costs and non-energy costs that are associated with ancillary services, such as reactive-power generation, voltage support, transient stability control, etc. Therefore, cost curves in the market-based OPF span more dimensions than their counterparts in the traditional OPF. For example, Figure 1.2 illustrates two curves for costing the voltage and phase angle difference.

- Longevity – Energy cost curves in the traditional OPF are mainly associated with fuel consumptions, and therefore, do not vary much in real-time operations. To the contrary, cost curves in the market-based OPF are driven by fluctuating offers and bids, which change at least on an hourly basis. As a result, the optimal dispatch may also change significantly from period to period in real-time operations, even if loads remain unchanged. Figure 1.3 demonstrates this phenomenon using a 30-bus power system example. As the degree of price fluctuation increases, the period-to-period dispatch change becomes increasingly constrained by generator ramping limits. Consequently, how the system is dispatched for the immediate next time period will not only determines the cost of operations for that single time period, but also affect the dispatches and cost of operations for several time periods further down the line. Therefore, the real-time market-based OPF must be formulated as a multi-period problem that takes into account generator ramping limits and costs of future operations, as opposed to the single-period problem in (1-1).

1.2.2 N-1 security constraints

Electric power systems, like any other critical infrastructures supporting modern
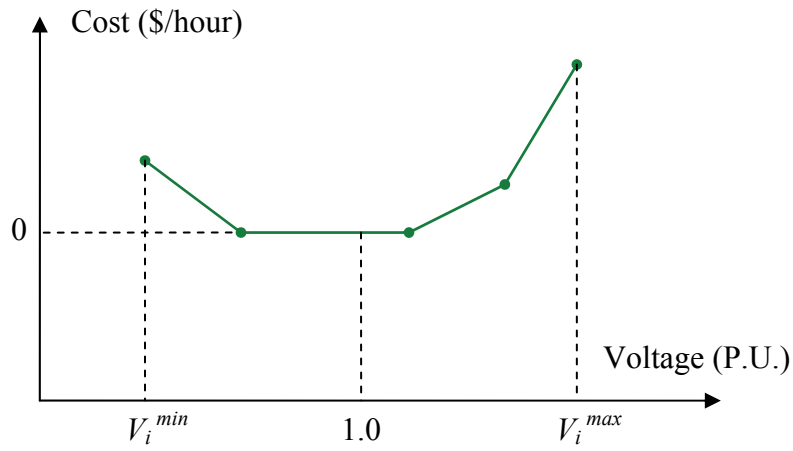
(a)
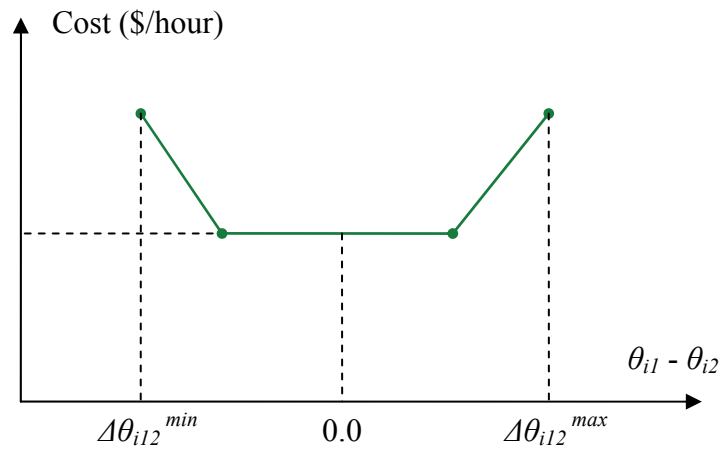
(b)

Figure 1.2 Example cost curves used in a market-based OPF for costing the voltage at a given bus and the phase angle difference between two buses: (a) a 4-segment piecewise linear voltage cost curve; (b) a 3-segment piecewise linear delta-angle cost curve.

Figure 1.3 Example optimal generator dispatches of a 30-bus 6-generator power system under different conditions: (a) a normalized 24-hour load curve showing the load changes assumed in the experiment; (b) optimal dispatches for four time periods 3:40 (green), 4:00 (blue), 16:40 (yellow), and 17:00 (red) under the static-cost condition, showing only small changes from period to period; (c) optimal dispatches at 3:40 (green), 4:00 (blue), 16:40 (yellow), and 17:00 (red) under the dynamic-cost condition (100% period-to-period fluctuations in energy offer prices), showing significant changes from period to period.
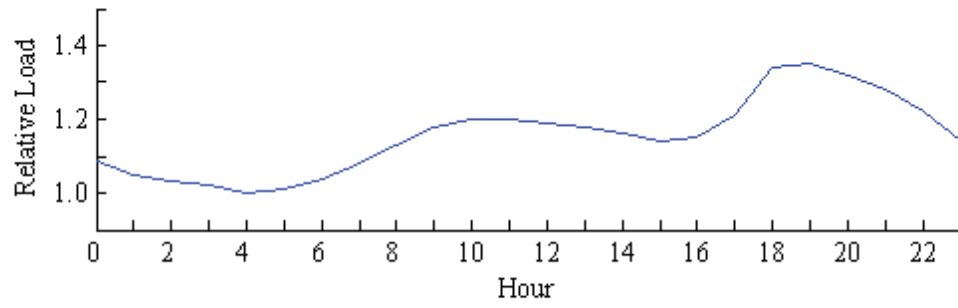
(a)
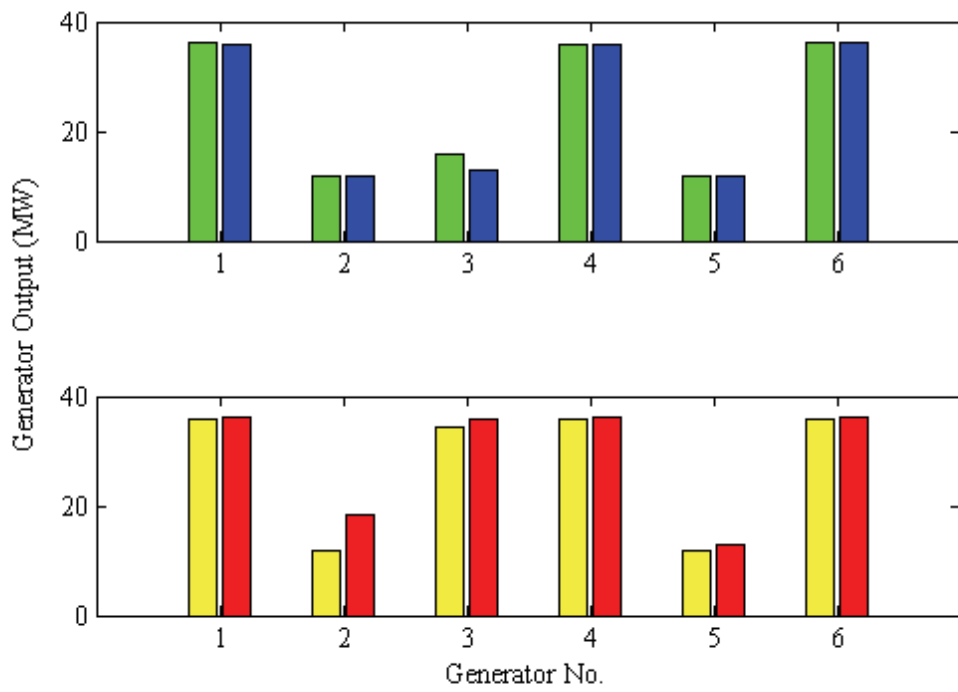
(b)

Figure 1.3 (Continued)
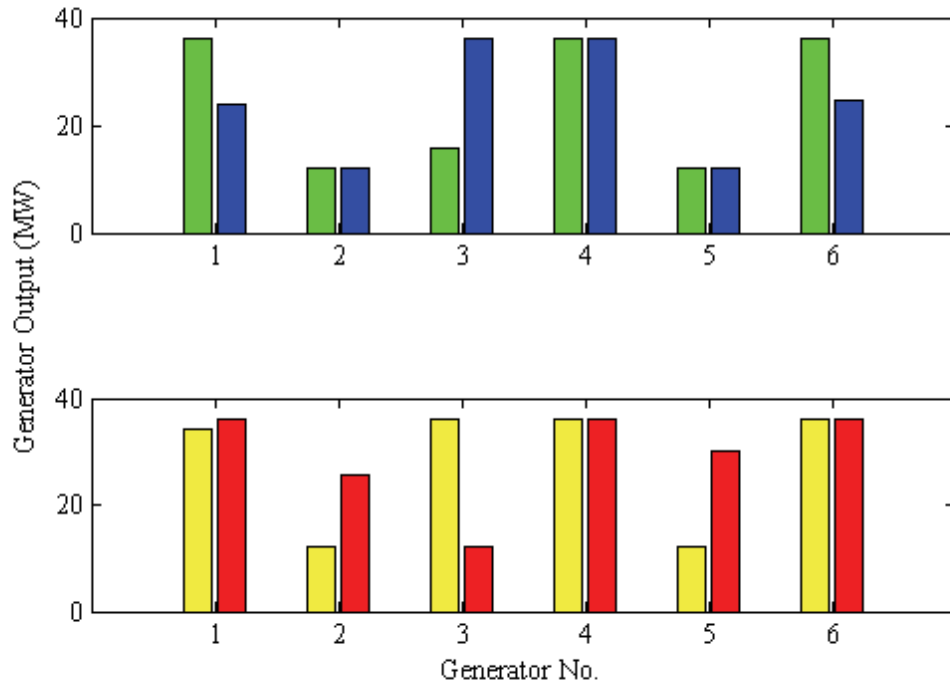
(c)

societies, must be designed and operated securely. The exact security rules being used vary from country to country and from operator to operator. The underlying principles, however, are the same and usually center around the so-called N-1 security requirement, i.e. to operate the system in a way that no single credible contingency (failure of a single bulk power facility or significant load change) can cause wide-spread system security problems, which typically include:

- Thermal limits violations

- Voltage instabilities

- Transient instabilities

Thermal limits are the most common constraints on transmission lines and transformers. Excessive power transfers across these devices can cause overheating, which will sag transmission lines, damage transformer insulations, and even trigger wide-spread cascading outages. In (1-1), these thermal limits are represented by the inequality constraints placed on pre-contingency branch power flows. Similarly, constraints limiting post-contingency branch flows with higher "emergency" limits can be added into the OPF formulation to represent the N-1 thermal security requirement, provided that post-contingency flows can be obtained directly (as functions of post-contingency control and states variables) or indirectly (through linear approximation around pre-contingency flows) in the extended OPF formulation.

Voltage instabilities stems from the attempt of load dynamics to restore power consumption beyond the capability of the combined generation and transmission systems after contingencies [43]. Transient instabilities arise from the loss of synchronism among machines due to contingencies [44]. An actuate assessment of voltage stabilities and transient stabilities requires tedious time-domain simulations of power systems dynamics, and is therefore impractical for integration with the real-time OPF. In practice, operators place pre-contingency or post-contingency surrogate

13

steady-state limits on voltages, transmission line flows, and phase angles to approximate the voltage and transient stability requirements [36-39].

In operating electricity markets, RTO's and ISO's need to integrate the above N-1 security constraints into their real-time security-constrained OPF's to obtain dispatches that are both economical and secure. Due to computational constraints and the lack of a clear regulatory definition of system security, however, different market operators have adopted different ways of implementing such SCOPF's.

At NYISO, post-contingency system states are modeled as being linearly dependent on pre-contingency states. Security constraints on these post-contingency states can thus be converted into constraints on pre-contingency states and added into the OPF through linear transformations. For example, to take into account contingencies that involve outages of transmission lines and/or generators, post-contingency real-power line flows are linearized through the use of power transfer distribution factors (PTDF) and generation shift factors (GSF), and get integrated into the OPF as

$$\left| R(V,\theta) + \begin{bmatrix} PTDF \\ GSF \end{bmatrix}^T \begin{bmatrix} \Delta R^{ci} \\ \Delta P^{ci} \end{bmatrix} \right| \le \min(R^{ci-\max}, S^{let-\max})$$

$$\Delta R_k^{ci} \equiv \begin{cases} R_k(V,\theta), & \text{if the loss of branch } k \text{ is part of contingency } ci \\ 0, & \text{otherwise} \end{cases} \quad , \quad (1\text{-}2)$$

$$\Delta P_j^{ci} \equiv \begin{cases} P_j, & \text{if the loss of generator } k \text{ is part of contingency } ci \\ 0, & \text{otherwise} \end{cases}$$

$$j \in [1, NG], \ k \in [1, NL], \ ci \in [1, NC]$$

where R represents real components of branch power flows, $R^{ci-\max}$ is the vector of proxy real branch-flow limits established for contingency ci, $S^{let-\max}$ is the vector of long-term emergency thermal limits placed on transmission lines and transformers, and NC stands for the number of contingencies. Obviously, the applicability of (1-2) is

limited, due to its lack of nonlinearity considerations pertaining to the reactive power flows, voltage stabilities, and transient stabilities.

At PJM, no post-contingency constraint appears in the OPF. Instead, a single set of pre-contingency surrogate limits derived from a comprehensive security analysis of all credible contingencies replace the original limits placed on voltages and branch power flows as

$$\max(V_i^{\text{pc-min}}, V_i^{\min}) \le V_i \le \min(V_i^{\text{pc-max}}, V_i^{\max})$$
$$|SF_k(V, \theta)| \le \min(S_k^{\text{pc-max}}, S_k^{\text{let-max}})$$
$$|ST_k(V, \theta)| \le \min(S_k^{\text{pc-max}}, S_k^{\text{let-max}})$$
$$i \in [1, NB], \ k \in [1, NL]$$

$\qquad$ (1-3)

where $V^{\text{pc-min}}$, $V^{\text{pc-max}}$, and $S^{\text{pc-max}}$ represents pre-contingency surrogate limits. In addition, pre-contingency limits $\Delta\theta^{\text{pc-min}}$ and $\Delta\theta^{\text{pc-max}}$ may be placed on phase angle differences among buses as

$$\Delta\theta_{i1,i2}^{\text{pc-min}} \le \theta_{i1} - \theta_{i2} \le \Delta\theta_{i1,i2}^{\text{pc-max}}$$
$$i1 \in [1, NB], \ i2 \in [1, NB]$$

$\qquad$ (1-4)

Such method takes into account all N-1 security constraints without increasing the complexity of the OPF. Yet, in using a single set of pre-contingency limits as opposed to multiple sets of post-contingency limits, (1-3) and (1-4) may over-constrain pre-contingency system states and lead to sub-optimal dispatches.

Variable duplication is another prominent way of integrating N-1 security constraints. In [2, 3, 5, 13-15, 29, 30, 34], a separate set of variables are created for each contingency case to represent the corresponding post-contingency system states. Post-contingency surrogate limits are then applied to those duplicated states. For example, to handle a branch-outage contingency, the duplicated variables and

constraints are added into the OPF as

$$FA_i^{ci}(P^{ci}, V^{ci}, \theta^{ci}) = 0$$

$$FR_i^{ci}(Q^{ci}, V^{ci}, \theta^{ci}) = 0$$

$$P_j^{ci} = P_j$$

$$VG_j^{ci} = VG_j$$

$$Q_j^{min} \leq Q_j^{ci} \leq Q_j^{max}$$

$$\max(V_i^{ci-min}, V_i^{min}) \leq V_i^{ci} \leq \min(V_i^{ci-max}, V_i^{max})$$

$$|SF_k^{ci}(V^{ci}, \theta^{ci})| \leq \min(S_k^{ci-max}, S_k^{let-max})$$

$$|ST_k^{ci}(V^{ci}, \theta^{ci})| \leq \min(S_k^{ci-max}, S_k^{let-max})$$

$$\Delta\theta_{i1,i2}^{ci-min} \leq \theta_{i1}^{ci} - \theta_{i1}^{ci} \leq \Delta\theta_{i1,i2}^{ci-max}$$

$$i \in [1, NB], \quad j \in [1, NG], \quad k \in [1, NL], \quad ci \in [1, NC]$$

$$i1 \in [1, NB], \quad i2 \in [1, NB] \tag{1-5}$$

where P^{ci}, Q^{ci}, V^{ci}, and θ^{ci} are the variables duplicated for contingency ci, VG^{ci} and VG represent the voltages at generator buses, FA^{ci}, FR^{ci}, SF^{ci}, and ST^{ci} represent nodal power balances and branch flows that take into account the system's status change under contingency ci, V^{ci-min}, V^{ci-max}, S^{ci-max}, $\Delta\theta^{ci-min}$, and $\Delta\theta^{ci-max}$ are post-contingency surrogate limits on voltages, branch flows, and phase angle differences. In (1-5), post-contingency states and pre-contingency states are tied together by the equality constraints placed on the control variables P, P^{ci}, VG, and VG^{ci}. Essentially, this preventive OPF formulation assumes that neither human interventions nor automatic control actions can take place in time to change the immediate post-contingency steady states once a contingency occurs. Compared to the first two OPF formulations described in this section, (1-5) reflects N-1 security requirements more accurately. It is, however, still far from being perfect. Most notably, it neglects the roles that AGC

generators play in post-contingency recoveries, and fails to consider the scenarios where generators run out of reactive power in response to contingencies. Besides, as one will see in later chapters, the couplings among pre-contingency variables and post-contingency variables introduce a large number of matrix fill-in's when the OPF problem is solved using Newton-like methods that involve direct sparse matrix factorizations, and the computational overhead associated with these matrix fill-in's makes it hard to solve any large-scale security-constrained OPF problem in real-time.

The SCOPF formulations discussed so far all assume that there is no time for the operator to conduct re-dispatches after the occurrence of a contingency. The power systems, however, are designed and operated with layers of margins. For example, short-term (15 ~ 30 minutes) emergency ratings of transmission lines are much higher than the normal and long-term (several hours) ones; surrogate limits for transient and voltage stabilities contain margins to account for the time (several minutes) that it takes for the systems to reach steady states. As a result, the operator will usually have enough time to do a re-dispatch after the occurrence of a contingency, as long as the solution of the SCOPF respects the security limits containing margins. This leads to another way of formulating SCOPF through variable duplications, i.e. eliminating the equality constraints tying pre-contingency and post-contingency control variables in (1-5) and replacing them with generator capacity limits or ramping limits (to be addressed in the next section) placed on post-contingency real and reactive power generations. This way of formulating SCOPF is more accurate and flexible. It is also easier to solve if one can accurately predict the binding generator ramping constraints and remove the non-binding ones.

1.2.3 Generator ramping limits

The scheduled output of a generator is often limited by its ramp rate, i.e. the speed at

which it can increase or decrease its real and reactive power generations. For most generators, the ramp rate is at least one percent of the generation capacity per minute [36, 37]. The unit commitment problem for day-ahead scheduling operations integrates generator ramping limits as

$$\max(P_{j,t-1} - RA_j \Delta T_D, P_j^{\min}) \le P_{j,t} \le \min(P_{j,t-1} + RA_j \Delta T_D, P_j^{\max})$$
$$j \in [1, NG], \ t \in [1, 24] \tag{1-6}$$

where $P_{j,t}$ is the real-power output of generator j during time period t, RA_j is the real-power ramp rate of generator j, and ΔT_D is the length (60 minutes) of a single time period in the day-ahead scheduling model. (1-6) couples the twenty-four hourly schedules, which are to be collectively optimized.

The OPF for real-time dispatching operations can model generator ramping limits in the same way as

$$\max(P_{j,t-1} - RA_j \Delta T_R, P_j^{\min}) \le P_{j,t} \le \min(P_{j,t-1} + RA_j \Delta T_R, P_j^{\max})$$
$$j \in [1, NG], \ t \in [t_0, t_0 + M] \tag{1-7}$$

where ΔT_R is the length (5-20 minutes) of a single time period in real-time dispatching operations, t_0 identifies the upcoming time period, and M is the number of additional future time periods to consider in deciding the dispatch for time period t_0. Existing real-time OPF's do not optimize multiple consecutive dispatches on a collective basis. Instead, they set M to zero and optimize the dispatch for the upcoming time period without any forward consideration of its impact on the optimality of future dispatches. Such simplification is somewhat ironic, given that generator ramping limits are more likely to be active and have effects on OPF solutions in real-time operations than in day-ahead scheduling operations. To take into account the couplings among dispatches for different time periods, one must solve a multi-period OPF that co-optimizes dispatches for the next $M+1$ periods in a look-ahead style. In such formulation, in

addition to (1-7), system states for each of the additional M periods are constrained in the same as they would be in a single-period standalone OPF. The objective function in (1-1) is replaced with:

$$\min_{P,Q,V,\theta} \quad \sum_{t=t0}^{t0+M} C(P_t,Q_t,V_t,\theta_t).$$
(1-8)

Essentially, as illustrated in Figure 1.4, the suggested formulation uses a sliding-window scheme that always requires the next dispatch to be optimized based on a "window" of forecasted future system conditions.

Figure 1.5 illustrates the difference between the cumulative cost of running 72 consecutive periods (24 hours) of real-time operations using standalone OPF's and that of running the same operations using 3-period look-ahead OPF's. Multi-period OPF's yield more economical solutions on a daily basis, for both the 30-bus system example and the 2383-bus system example. In Figure 1.6, one can see that the overall daily operations cost decreases as the size of the look-ahead window M increases. For the 30-bus system, no further improvement is observed for M beyond 3. Although the cost improvement that multi-period OPF's provide is small (single-digit) in percentage terms, it is quite significant by the industry's standards and very large in dollar terms. To put it into perspectives, on the day of April 19, 2007, one percent of the daily operations cost of PJM roughly amounts to one million US dollars. Appendix B gives a more detailed comparison of the operations costs, dispatches, and LMPs generated by standalone OPF's and those by multi-period OPF's using a 3-bus system example.

1.2.4 A comprehensive formulation of real-time market-based OPF

In light of the above analysis, a comprehensive real-time market-based OPF is formulated as
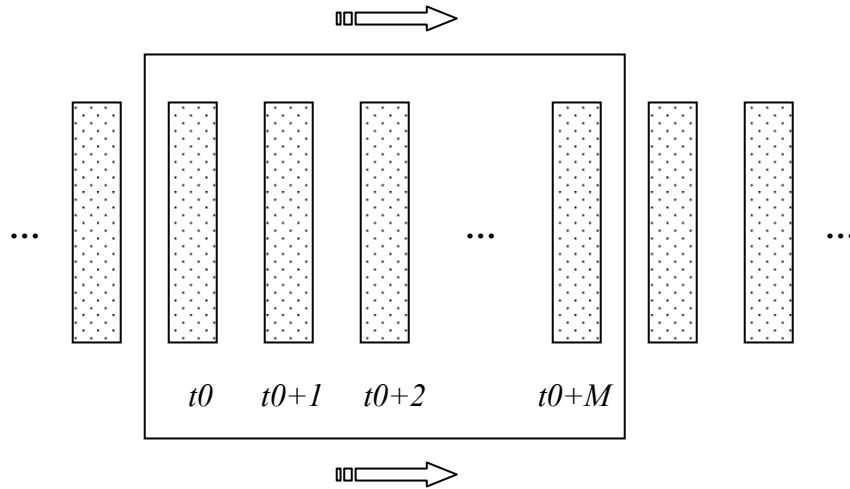
Figure 1.4 Illustration of the sliding-window scheme used in the multi-period OPF. Each bar represents a whole set of system states, costs, and constraints related to the standalone dispatch optimization for that period. The sliding box (window) spans $M+1$ periods (one upcoming period and M look-ahead periods) and moves from left to right one block at a time. At time $t0$, it contains all information that goes into the multi-period OPF to be solved for the upcoming dispatch.

Figure 1.5 Illustration of the growing difference between the cumulative cost of running real-time operations using standalone OPF's and that of running real-time operations using 3-period look-ahead OPF's: (a) 72-period (24-hour) cumulative cost differences for a 30-bus system; (b) 72-period (24-hour) cumulative cost differences for a 2383-bus system. Positive differences indicate that multi-period OPF's offer cost savings. The experiment adopts the same load profile as used in Figure 1.3, assumes 100% period-to-period fluctuations in energy offer prices, and set the ramping limit *RA* of each generator to be 1% of the generator's capacity per minute.
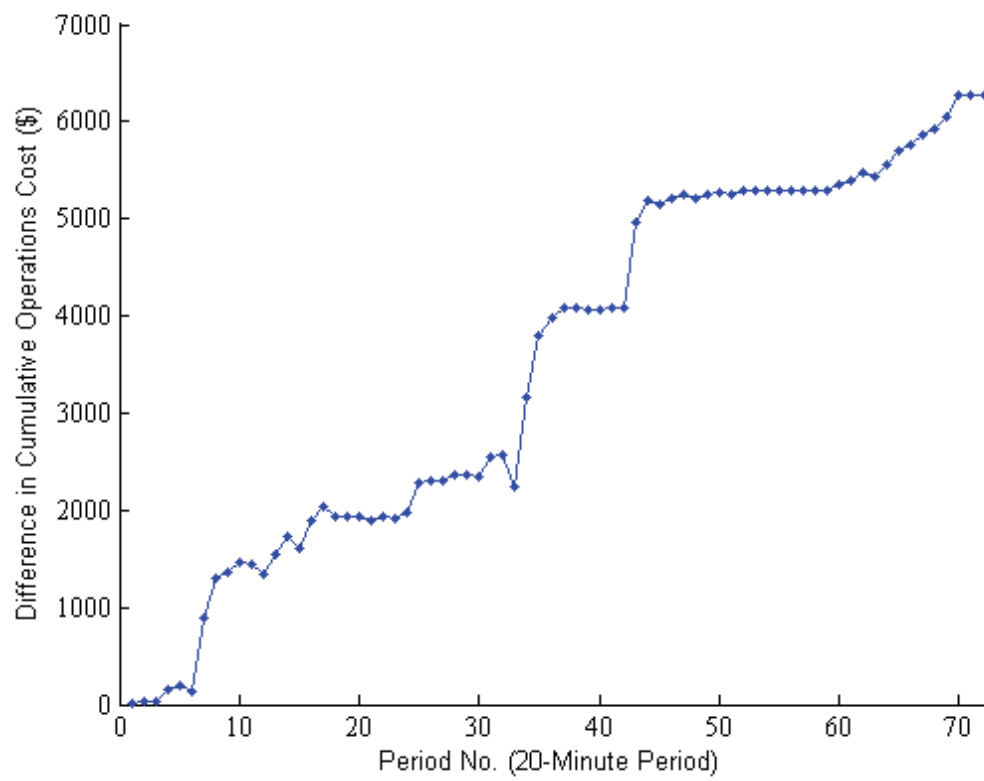
(a)

Figure 1.5 (Continued)
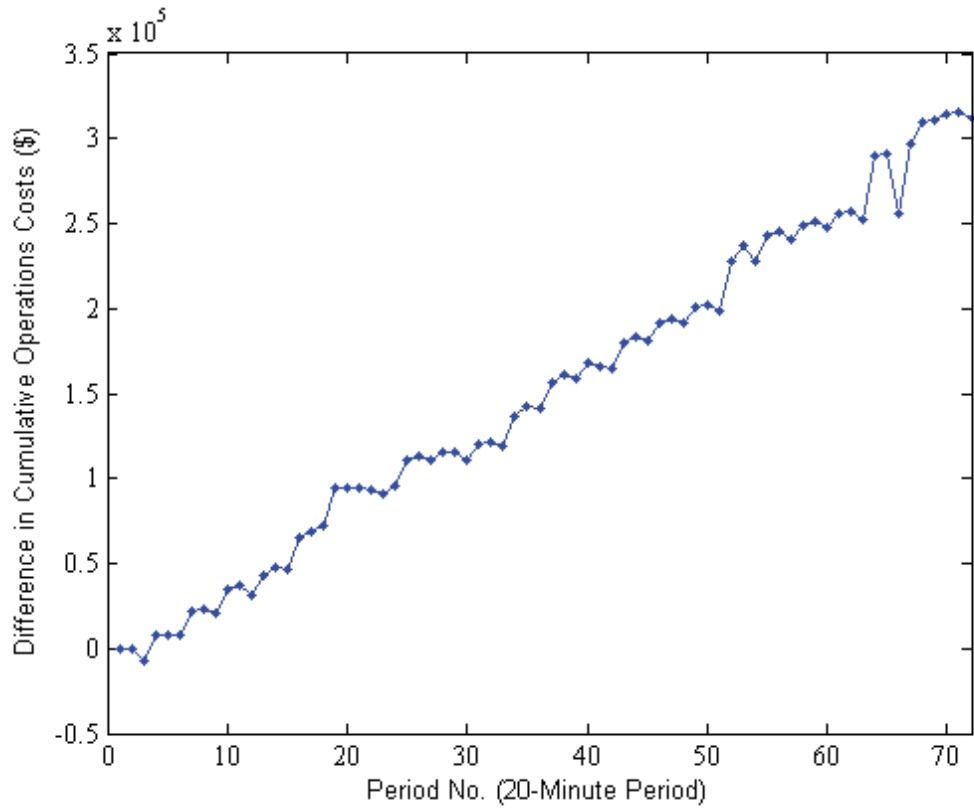
(b)
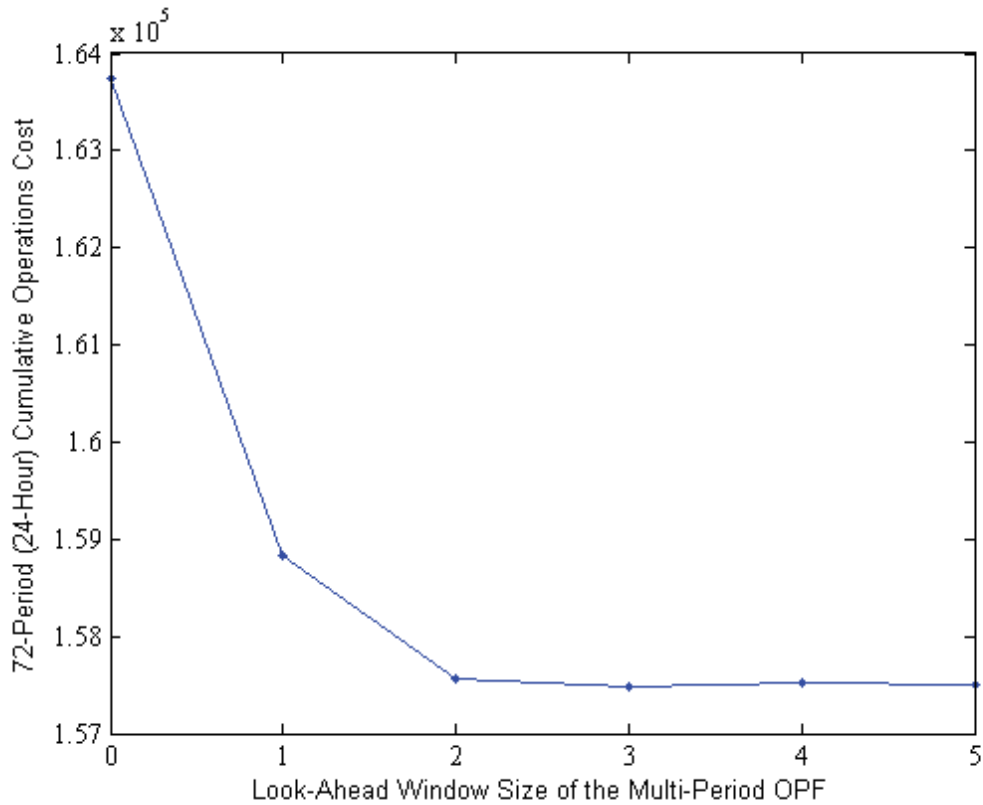
Figure 1.6 Cumulative costs of running 72-period (24-hour) real-time operations with multi-period OPF's that adopt different look-ahead sizes. The experiment adopts the same 30-bus system model and load profile as used in Figure 1.3, assumes 100% period-to-period fluctuations in energy offer prices, and set the ramping limit *RA* of each generator to be 1% of the generator's capacity per minute.

$$\min_{P,Q,V,\theta} \sum_{t=t0}^{t0+M} C_t(P_t,Q_t,V_t,\theta_t)$$

s.t. $FA_{i,t}(P_t,V_t,\theta_t)=0$

$FR_{i,t}(Q_t,V_t,\theta_t)=0$

$\max(P_{j,t-1}-ra_{j,t}\Delta T_R,P_j^{\min}) \le P_{j,t} \le \min(P_{j,t-1}+ra_{j,t}\Delta T_R,P_j^{\max})$

$\max(Q_{j,t-1}-rr_{j,t}\Delta T_R,Q_j^{\min}) \le Q_{j,t} \le \min(Q_{j,t-1}+rr_{j,t}\Delta T_R,Q_j^{\max})$

$ra_{j,t}+rr_{j,t} \le RS_j$

$V_i^{\min} \le V_{i,t} \le V_i^{\max}$

$|SF_k(V_t,\theta_t)| \le S_k^{\text{nt}-\max}$

$|ST_k(V_t,\theta_t)| \le S_k^{\text{nt}-\max}$

$FA_{i,t}^{ci}(P_t^{ci},V_t^{ci},\theta_t^{ci})=0$

$FR_{i,t}^{ci}(Q_t^{ci},V_t^{ci},\theta_t^{ci})=0$

$\max(P_{j,t}-ra_{j,t}^{ci}\Delta T_R,P_j^{\min}) \le P_{j,t}^{ci} \le \min(P_{j,t}+ra_{j,t}^{ci}\Delta T_R,P_j^{\max})$

$\max(Q_{j,t}-rr_{j,t}^{ci}\Delta T_R,Q_j^{\min}) \le Q_{j,t}^{ci} \le \min(Q_{j,t}+rr_{j,t}^{ci}\Delta T_R,Q_j^{\max})$

$ra_{j,t}^{ci}+rr_{j,t}^{ci} \le RS_j$

$\max(V_{i,t}^{ci-\min},V_i^{\min}) \le V_{i,t}^{ci} \le \min(V_{i,t}^{ci-\max},V_i^{\max})$

$|SF_k^{ci}(V_t^{ci},\theta_t^{ci})| \le \min(S_{k,t}^{ci-\max},S_k^{\text{let}-\max})$

$|ST_k^{ci}(V_t^{ci},\theta_t^{ci})| \le \min(S_{k,t}^{ci-\max},S_k^{\text{let}-\max})$

$\Delta\theta_{i1,i2,t}^{ci-\min} \le \theta_{i1,t}^{ci}-\theta_{i2,t}^{ci} \le \Delta\theta_{i1,i2,t}^{ci-\max}$

$i \in [1,NB],\ j \in [1,NG],\ k \in [1,NL],\ i1 \in [1,NB],\ i2 \in [1,NB]$

$ci \in [1,NC],\ t \in [t_0,t_0+M]$

, (1-9)

where generator ramping limits *RS* are placed on the aggregates of real and reactive

power ramp rates *ra* and *rr*. When only real-power ramping limits are considered, the

comprehensive real-time market-based OPF problem is written as

$$\min_{P,Q,V,\theta} \sum_{t=t0}^{t0+M} C_t(P_t,Q_t,V_t,\theta_t)$$

$$\text{s.t.} \quad FA_{i,t}(P_t,V_t,\theta_t) = 0$$

$$FR_{i,t}(Q_t,V_t,\theta_t) = 0$$

$$\max(P_{j,t-1} - RA_j\Delta T_R, P_j^{\min}) \leq P_{j,t} \leq \min(P_{j,t-1} + RA_j\Delta T_R, P_j^{\max})$$

$$Q_j^{\min} \leq Q_{j,t} \leq Q_j^{\max}$$

$$V_i^{\min} \leq V_{i,t} \leq V_i^{\max}$$

$$| SF_k(V_t,\theta_t) | \leq S_k^{nt-\max}$$

$$| ST_k(V_t,\theta_t) | \leq S_k^{nt-\max}$$

$$FA_{i,t}^{ci}(P_t^{ci},V_t^{ci},\theta_t^{ci}) = 0$$

$$FR_{i,t}^{ci}(Q_t^{ci},V_t^{ci},\theta_t^{ci}) = 0$$

$$\max(P_{j,t} - RA_j\Delta T_R, P_j^{\min}) \leq P_{j,t}^{ci} \leq \min(P_{j,t} + RA_j\Delta T_R, P_j^{\max})$$

$$Q_j^{\min} \leq Q_{j,t}^{ci} \leq Q_j^{\max}$$

$$\max(V_{i,t}^{ci-\min},V_i^{\min}) \leq V_{i,t}^{ci} \leq \min(V_{i,t}^{ci-\max},V_i^{\max})$$

$$| SF_k^{ci}(V_t^{ci},\theta_t^{ci}) | \leq \min(S_{k,t}^{ci-\max}, S_k^{let-\max}) \tag{1-10}$$

$$| ST_k^{ci}(V_t^{ci},\theta_t^{ci}) | \leq \min(S_{k,t}^{ci-\max}, S_k^{let-\max})$$

$$\Delta\theta_{i1,i2,t}^{ci-\min} \leq \theta_{i1,t}^{ci} - \theta_{i2,t}^{ci} \leq \Delta\theta_{i1,i2,t}^{ci-\max}$$

$$i \in [1, NB], \quad j \in [1, NG], \quad k \in [1, NL], \quad i1 \in [1, NB], \quad i2 \in [1, NB]$$

$$ci \in [1, NC], \quad t \in [t_0, t_0 + M]$$

The solution of (1-10) is the central theme of the rest of this work. The methods discussed will be applicable to the solution of (1-9) as well.

Hereinafter, the generator ramping constraints established among variables

representing system states for different time periods,

$$\max(P_{j,t-1} - RA_j \Delta T_R, P_j^{\min}) \leq P_{j,t} \leq \min(P_{j,t-1} + RA_j \Delta T_R, P_j^{\max}),$$

are referred as the time-coupling constraints, or simply the time-couplings, while the ramping constraints established among variables representing system states for different pre-contingency and post-contingency cases,

$$\max(P_{j,t} - RA_j \Delta T_R, P_j^{\min}) \leq P_{j,t}^{ci} \leq \min(P_{j,t} + RA_j \Delta T_R, P_j^{\max}),$$

are referred as the contingency-coupling constraints or the contingency-couplings.

1.3 Nonlinear programming techniques

For most real-size power systems, the problem formed in (1-10) is a large-scale constrained nonlinear optimization problem. Over the past two decades, research on large-scale nonlinear programming has proliferated. Among the techniques developed, augmented Lagrangian methods (ALM) are most reliable and usable for solving general-purpose constrained optimization problems [45]. Yet, their reliabilities largely depend on what methods are used to solve the converted unconstrained optimization problems. Trust-region methods (TRM) represent the state-of-the-art of globally convergent unconstrained optimizations [46-50]. Surprisingly, the combined use of TRM and ALM has not been reported in the power system community. In fact, there has been no mention of trust-region methods in any OPF literature, probably in part due to the timely introduction of more efficient primal-dual interior point methods (PDIPM). PDIPM is a major development that has merged LP and NLP. It resulted in a reassessment of how constraints are treated in NLP [51, 52]. For most nonlinear optimization problems, PDIPM achieves great computational efficiency, but often at the cost of losing the global convergence guarantee.

This section briefly reviews the NLP methods mentioned above, in preparation for later discussions on new OPF formulations and algorithms.

1.3.1 Augmented Lagrangian methods

In solving a constrained optimization problem of the form

$$\min_{X} \quad f(X)$$

$$\text{s.t.} \quad H(X) = 0, \quad\quad\quad\quad\quad\quad\quad (1\text{-}11)$$

$$G(X) \leq 0$$

augmented Lagrangian methods convert the problem into a sequence of unconstrained optimization problems with penalty terms. For example, using quadratic penalties and squared slack variables, (1-11) can be converted into an iterative series of

$$\min_{X^k, Z^k} L^k(X^k, Z^k, \lambda^k, \mu^k) = f(X^k) + (\lambda^k)^T H(X^k) + \frac{1}{2} H(X^k)[W^k] H(X^k)$$

$$+ \sum_{m=1}^{ni} \{ \mu_m^k [G_m(X^k) + (Z_m^k)^2] + \frac{U_m^k}{2} \mid G_m(X^k) + (Z_m^k)^2 \mid^2 \} \quad , \quad (1\text{-}12)$$

which is equivalent to

$$\min_{X^k} L_R{}^k(X^k, \lambda^k, \mu^k) = f(X^k) + (\lambda^k)^T H(X^k) + \frac{1}{2} H(X^k)[W^k] H(X^k)$$

$$\quad\quad\quad\quad\quad\quad\quad (1\text{-}13)$$

$$+ \sum_{m=1}^{ni} \frac{1}{2 U_m^k} \{ \max[0, \mu_m^k + U_m^k G_m(X^k)]^2 - (\mu_m^k)^2 \}$$

after the minimization with respect to the slack variables Z^k in iteration k. In (1-12) and (1-13), λ^k and μ^k are Lagrange multipliers, W^k and U^k are penalty parameters, and ni is the number of inequality constraints. In the so-called "multiplier method", λ^k, μ^k, W^k, and U^k are updated after each iteration of unconstrained optimization as

$$\lambda^{k+1} = \lambda^k + [W^k]H(X^k)$$

$$\mu_m^{k+1} = \max[0, \mu_m^k + U_m^k G_m(X^k)]$$

$$W_r^{k+1} = \begin{cases} \beta_W W_r^k & \text{if } |H_r(X^k)| > \gamma_W |H_r(X^{k-1})| \\ W_r^k & \text{if } |H_r(X^k)| \le \gamma_W |H_r(X^{k-1})| \end{cases}, \tag{1-14}$$

$$U_m^{k+1} = \begin{cases} \beta_U U_m^k & \text{if } G_m(X^k) > \gamma_U G_m(X^{k-1}) \\ U_j^k & \text{if } G_m(X^k) \le \gamma_U G_m(X^{k-1}) \end{cases}$$

where $0 < \gamma_W, \gamma_U < 1$ and $\beta_W, \beta_U > 1$ are constants, and r is the equality constraint index. Convergence is achieved when

$$\| \nabla_{X^k} L_R^k(X^k, \lambda^k, \mu^k) \| \le \varepsilon^k$$

$$\frac{\| \lambda^{k+1} - \lambda^k \|}{1 + \| \lambda^k \|_\infty} \le \varepsilon_\lambda \tag{1-15}$$

$$\frac{\| \mu^{k+1} - \mu^k \|}{1 + \| \mu^k \|_\infty} \le \varepsilon_\mu$$

are satisfied. In (1-15), ε_λ and ε_μ are two constant tolerance parameters that are greatly less than one, and the variable tolerance parameter ε^k decreases to a near-zero value ε^∞ as the iteration number k increases. Combined with a suitable unconstrained optimization algorithm, the above augmented Lagrangian method solves large-scale nonlinear constrained optimization problems very reliably.

1.3.2 Trust-region methods

Trust-region methods represent a category of globally convergent unconstrained optimization algorithms. In solving an unconstrained optimization problem

$$\min_X f(X) \tag{1-16}$$

using the Newton's method, each pure Newton step is obtained by minimizing over S

the second-order Taylor series approximation of f around the trial solution X^k, given by

$$f^k(S) = f(X^k) + \nabla f(X^k)^T S + \frac{1}{2} S^T \nabla^2 f(X^k) S.$$ (1-17)

The problem with the Newton's method is that the iterative step S is not always on the descent direction because it often lies outside the small neighborhood where the approximation in (1-17) stays valid. Trust region methods address this issue by using a restricted Newton step S^k obtained from the minimization of $f^k(S)$ over a small neighborhood Δ^k, the trust region, as

$$S^k = \arg \min_{\|S\| \leq \Delta^k} f^k(S).$$ (1-18)

It is known that the restricted Newton step S^k is essentially a solution of

$$(\nabla^2 f(X^k) + \alpha^k I)S = -\nabla f(X^k),$$ (1-19)

where I is the identity matrix and α^k is a nonnegative scalar. Trust region methods can therefore be viewed as a special category of damped Newton's methods. In order to maintain the trustworthy of the trust region, one needs to check the validity of the Taylor series approximation within the region Δ^k, and adjust Δ^k if necessary. Algorithm 1.1 illustrates how this is done in the context of solving (1-16) using a classic trust-region method.

To solve the sub-problem in (1-18) and (1-19), [47] applied the Newton procedure to solve for α^k in:

$$\phi(\alpha^k) \equiv \frac{1}{\Delta^k} - \frac{1}{\| S(\alpha^k) \|} = 0$$ (1-20)
$$S(\alpha^k) \equiv -(\nabla_X^2 f(X^k) + \alpha^k I)^{-1} \nabla_X f(X^k)$$

This computation typically involves several rounds of Cholesky factorizations of the damped Hessian matrix of $f(X)$.

Algorithm 1.1

Let $0 < \tau < \eta < 1$, $0 < \gamma_1 < 1 < \gamma_2$, $\Delta^0 > 0$, and X^0 be given,

$k = 0$

while $\| \nabla_X f(X^k) \| > \varepsilon$ **do**

$$\psi^k(S) \equiv \nabla_X f(X^k)^T S + \frac{1}{2} S^T \nabla_X^2 f(X^k) S$$

$$S^k = \arg \min_{\|S\| \leq \Delta^k} \psi^k(S)$$

$$\rho^k = \frac{f(X^k + S^k) - f(X^k)}{\psi^k(S^k)}$$

if $\rho^k > \tau$

$$X^{k+1} = X^k + S^k$$

else

$$X^{k+1} = X^k$$

end if

if $\rho^k \leq \tau$

$$\Delta^{k+1} = \gamma_1 \| S^k \|$$

else if $\rho^k > \eta$ **and** $\| S^k \| == \Delta^k$

$$\Delta^{k+1} = \gamma_2 \Delta^k$$

else

$$\Delta^{k+1} = \Delta^k$$

end if

$k = k + 1$

end do

To reduce the computation overhead, Coleman et al. proposed a two-dimensional trust-region method for solving large-scale optimization problems [48, 49]. In their proposed method, the trust region formed by $||S|| \leq \Delta^k$ in (1-18) is replaced by a two-dimensional region that spans the gradient direction and the direction generated by a modified PCG or Cholesky procedure. Nevertheless, our experiments show that neither the PCG nor the Cholesky variation of this 2-D trust-region method is able to solve large-scale OPF problems without running into numerical difficulties.

1.3.3 Primal-dual interior point methods

The primal-dual interior point method (PDIPM) and its many variations have become the algorithms of choice for solving OPF's over the past decade [7-13]. PDIPM relates to the barrier method, which formulates the Lagrangian of (1-11) as

$$L^{\gamma}(X,Z,\lambda,\mu) \equiv f(X) + \lambda^T H(X) + \mu^T (G(X) + Z) - \gamma \sum_{m=1}^{ni} \ln(Z_m), \qquad (1\text{-}21)$$

where γ is a positive scalar and Z is the vector of positive slack variables. The first-order Karush-Kuhn-Tucker (KKT) condition of (1-21) is written as

$$\nabla_X L^{\gamma}(X,Z,\lambda,\mu) = 0$$
$$H(X) = 0$$
$$G(X) + Z = 0 \qquad , \qquad (1\text{-}22)$$
$$[\mu]Z - \gamma e = 0$$
$$Z > 0, \ \mu > 0$$

where e is the unitary vector and $[\ldots]$ diagonalizes the enclosed vector. The Newton's method can be used to solve (1-22). Each Newton step involves the solution of

$$\begin{bmatrix} \nabla^2_{xx}L^\gamma(X,Z,\lambda,\mu) & 0 & \nabla H(X) & \nabla G(X) \\ 0 & [\frac{\mu}{Z}] & 0 & I \\ \nabla H(X)^T & 0 & 0 & 0 \\ \nabla G(X)^T & I & 0 & 0 \end{bmatrix} \begin{bmatrix} \Delta X \\ \Delta Z \\ \Delta\lambda \\ \Delta\mu \end{bmatrix} = \begin{bmatrix} -\nabla_X L^\gamma(X,Z,\lambda,\mu) \\ -(\mu-\gamma[Z]^{-1}e) \\ -H(X) \\ -G(X)-Z \end{bmatrix}, \quad (1\text{-}23)$$

which can be reduced into

$$\Delta Z = -G(X) - Z - \nabla G(X)^T \Delta X$$

$$\Delta\mu = -\mu + [Z]^{-1}(\gamma e - [\mu]\Delta Z)$$

$$\begin{bmatrix} M & \nabla H(X) \\ \nabla H(X)^T & 0 \end{bmatrix} \begin{bmatrix} \Delta X \\ \Delta\lambda \end{bmatrix} = \begin{bmatrix} -N \\ -H(X) \end{bmatrix} \qquad (1\text{-}24)$$

$$M \equiv \nabla^2_{XX}L^\gamma(X,Z,\lambda,\mu) + \nabla G(X)[Z]^{-1}[\mu]\nabla G(X)^T$$

$$N \equiv \nabla_X L^\gamma(X,Z,\lambda,\mu) + \nabla G(X)[Z]^{-1}([\mu]G(X) + \gamma e)$$

The barrier method and PDIPM maintain the strict feasibility of the trial solution by truncating the Newton step according to

$$\alpha_p = \min(\xi \min_{\Delta Z_m < 0}(-Z_m/\Delta Z_m), 1)$$

$$\alpha_d = \min(\xi \min_{\Delta\mu_m < 0}(-\mu_m/\Delta\mu_m), 1)$$

$$X = X + \alpha_p \Delta X$$

$$Z = Z + \alpha_p \Delta Z \qquad , \qquad (1\text{-}25)$$

$$\lambda = \lambda + \alpha_d \Delta\lambda$$

$$\mu = \mu + \alpha_d \Delta\mu$$

where ξ is a constant scalar marginally less than one. When γ is zero, (1-22) becomes the first-order KKT condition of the original optimization problem (1-11). In PDIPM, γ is called the parameter of perturbation and must converge to zero during the Newton-like iterations. One way of setting γ is through the use of the primal-dual distance, which is defined for the mth inequality constraint as the product of $G_m(X)$ and μ_m. For

example,

$$\gamma = \sigma(\mu^T Z)/ni \qquad\qquad\qquad (1\text{-}26)$$

ties γ to the average of distances from the current solution to the optimal point. The constant σ, referred to as the parameter of the direction combination, satisfies $0 < \sigma < 1$ and defines the trajectory to the optimal solution by combining the affine-scaling direction ($\sigma = 0$) and the centralization direction ($\sigma = 1$).

Other PDIPM variants, such as the predictor-corrector interior point method, improve the performance by reducing the number of matrix factorizations at the cost of increased number of iterations [8]. The overall complexities of these variants, however, remain the same.

The classic PDIPM algorithm described above is not globally convergent, because it only concerns the first-order KKT condition. Studies reported in [12, 51] seek to improve the convergence through line searching and damped Newton procedures. The desired property of global convergence, however, comes at the cost of performance.

1.4 Nonsmooth optimizations

The term "nonsmooth" refers to situations in which smoothness (or differentiability) is not postulated [53]. An optimization problem is nonsmooth if its objective function or any of its constraints is nonsmooth. The piecewise cost function in the OPF is a natural source of nonsmoothness, as shown in Figure 1.1 and 1.2. Traditional NLP algorithms described in the previous section are built on smoothness assumptions and therefore cannot be extended to solve nonsmooth optimization problems directly. The gradients and Hessians that these algorithms depend on do not even exist at the breakpoints of piecewise functions. The study in [53] provides a theoretical

framework for nonsmooth analysis using generalized gradients and generalized Jacobians. The market-based OPF problem with piecewise costs is a Class-5 composite nonsmooth problem [54], i.e. the nonsmooth objective function is made up piecewise from a finite number of smooth functions, and its generalized gradients and Hessians at any given point can be evaluated directly from the underlying smooth functions. There are two categories of methods available for the solution of Class-5 problems. In the first one, algorithmic techniques are tailored to the composite nonsmooth optimization. In the second one, reformulations are carried out to transform nonsmooth optimization problems into equivalent or approximately equivalent smooth optimization problems. With the maturity of constrained nonlinear programming, the reformulation approach has become more attractive and shall be the focus of this study. In the section below, Class-5 composite nonsmooth optimization problems are further classified into several sub-categories. Relevant nonsmooth optimization techniques are then reviewed.

1.4.1 Further classification of Class-5 problems

Class-5 composite nonsmooth optimization problems can be further classified into eight categories listed in Table 1.1 according to three tests:

- I – Whether the piecewise portion of the objective function is strictly convex;
- II – Whether the piecewise portion of the objective function is linear;
- III – Whether the problem is in a minimax form.

A Class-5 problem is a minimax problem if its is in the form of

$$\min_{X \in R^n} f(X) \equiv \max_{s=1,\dots,d} f_s(X), \tag{1-27}$$

where f_s's are smooth functions. It is easy to see that, if a Class-5 problem passes Test II, it will either pass both of the other two tests or fail both. Hence, Category 2 and 5

35

Table 1.1 Eight categories of Class-5 composite nonsmooth optimization problems classified according the three tests on convexity, piecewise linearity, and minimax conformity. The categories marked with "Phantom" contain no meaningful problem.

Category	Test I	Test II	Test III
1	Yes	Yes	Yes
2 (Phantom)	Yes	Yes	No
3	Yes	No	Yes
4	Yes	No	No
5 (Phantom)	No	Yes	Yes
6	No	Yes	No
7	No	No	Yes
8	No	No	No

listed in Table 1.1 are phantom categories that do not need further considerations.

The OPF problems constructed with the cost curves shown in Figure 1.1 and 1.2 belong to Category 1. Figure 1.7 shows example objective functions from the other five non-phantom categories. These functions do not necessarily reflect costing schemes used in today's market operations; but they represent some potential ways of improving the costing flexibility and versatility for future markets. For simplicity, hereinafter, the underlying optimization problem is assumed to consist of only one piecewise function and is to be solved in a one-dimensional space.

1.4.2 Separable programming approach

For a smooth nonlinear optimization problem in the form of

$$\min \ f(x)$$
$$\text{s.t.} \ \ h_r(x) = 0 \quad \text{for } r = 1,...,ne, \tag{1-28}$$
$$g_m(x) \leq 0 \quad \text{for } m = 1,...,ni$$

the separable programming method approximates $f(x)$, $h_r(x)$'s, and $g_m(x)$'s with piecewise linear functions and restates the problem as

$$\min \ \sum_{v=1}^{ns+1} \lambda_v f(x_v)$$

$$\text{s.t.} \ \ \sum_{v=1}^{ns+1} \lambda_v h_r(x_v) = 0 \quad \text{for } r = 1,...,ne$$

$$\sum_{v=1}^{ns+1} \lambda_v g_m(x_v) \leq 0 \quad \text{for } m = 1,...,ni \tag{1-29}$$

$$\sum_{v=1}^{ns+1} \lambda_v = 1$$

$$\lambda_v \geq 0 \quad \text{for } v = 1,...,ns+1$$

At most, two adjacent λ_v's are positive

Figure 1.7 Illustration of example objective functions of Class-5 composite nonsmooth optimization problems in Category 3, 4, 6, 7 and 8: (a) Category-3 objective function generated from two reciprocal functions and one linear function; (b) Category-4 objective function generated from two quadratic functions and one linear function; (c) Category-6 objective function generated from three linear functions; (d) Category-7 objective function generated from two reciprocal functions and one linear function; (e) Category-8 objective function generated from two linear functions and one quadratic function.
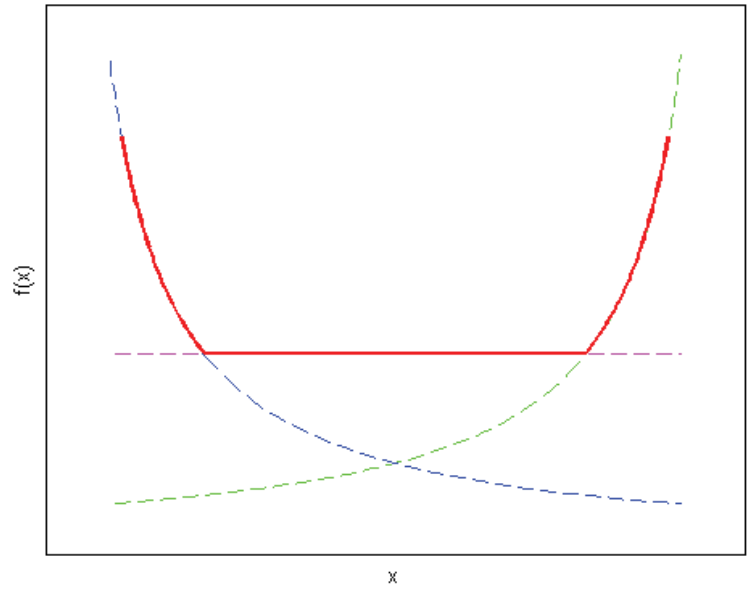
(a)
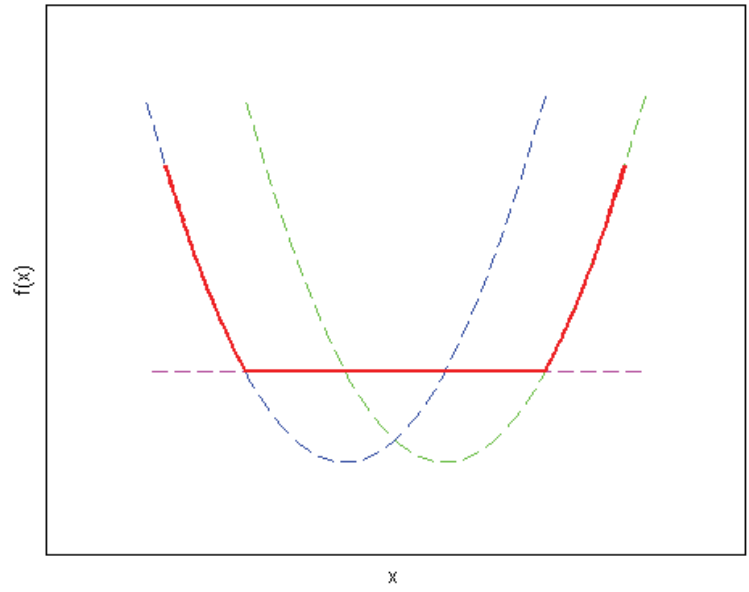
(b)

Figure 1.7 (Continued)
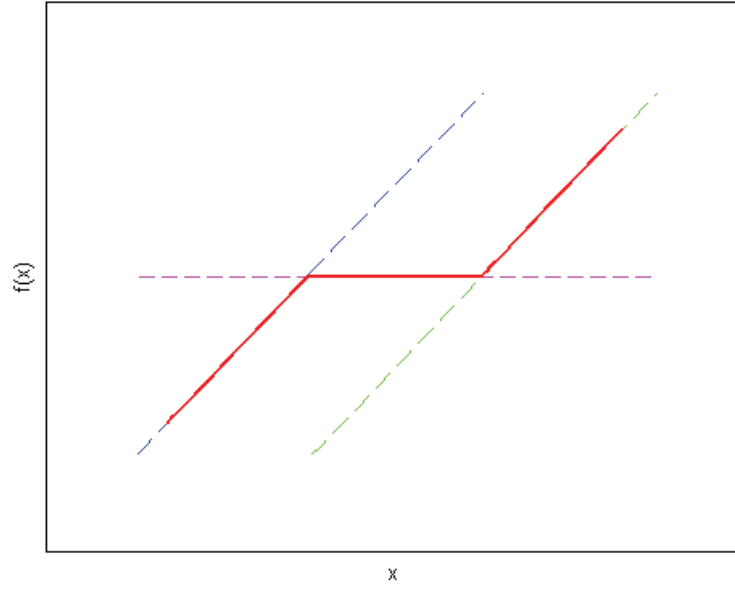
(c)
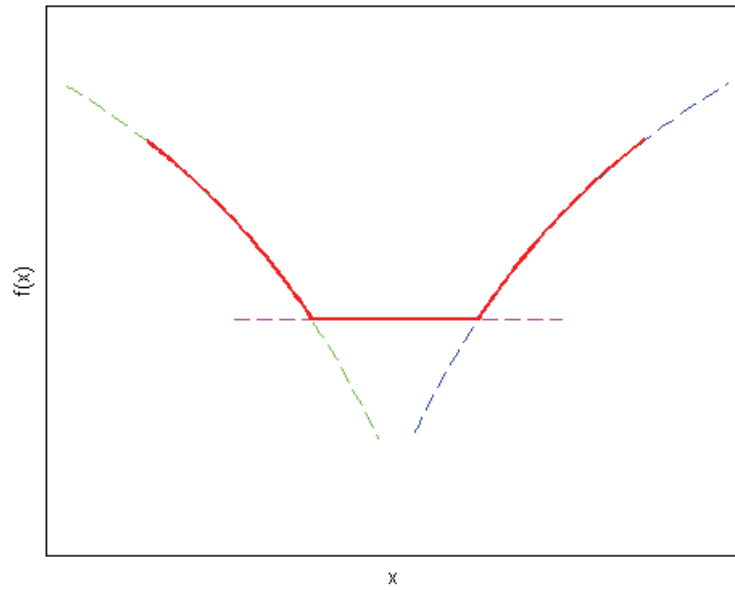
(d)

Figure 1.7 (Continued)
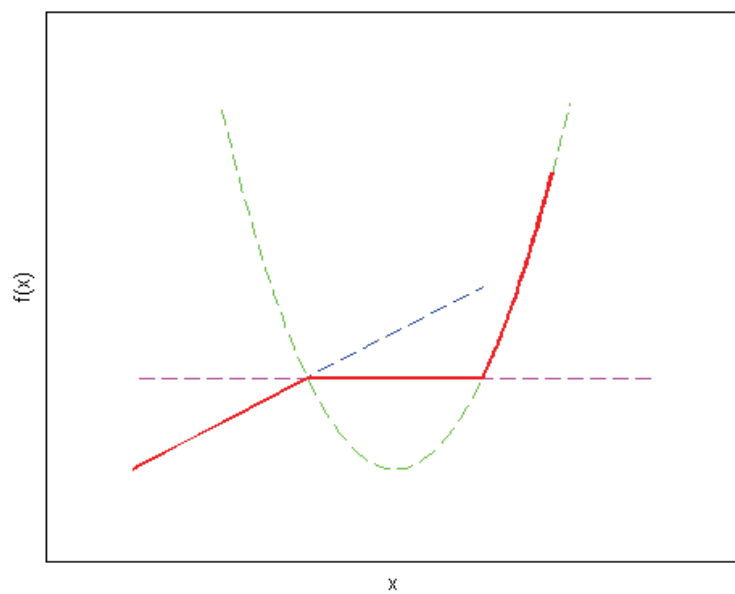
(e)

where ns is the number of segments contained in each piecewise linear function, and x_v's are the $ns+1$ distinctive values of x at the breakpoints of the piecewise linear functions [55]. Assuming x_v's are uniformly spread, the larger the ns, the better (1-29) approximates (1-28). The adjacency constraint at the end of (1-29) complicates the solution of the problem. When $h_r(x)$'s and $g_m(x)$'s are convex and $f(x)$ is strictly convex, however, this adjacency constraint can be safely removed. Problem (1-29) without the adjacency constraint is a smooth LP problem and can be easily solved. The accuracy of the smooth programming method greatly depends on the granularity of the linearization. Formulating and solving (1-29) with a larger ns yields a solution closer to that of (1-28), but consumes more memory and computation time due to the overhead associated with more variables and constraints.

The reformulation technique above can be borrowed to handle some of the Class-5 composite nonsmooth optimization problems. Suppose now that $f(x)$ in (1-28) is already a piecewise linear function, as opposed to a smooth function, while $h_r(x)$'s and $g_m(x)$'s are smooth functions, one can reformulate the problem as

$$\min \sum_{v=1}^{ns+1} \lambda_v f(x_v)$$

$$\text{s.t.} \quad h_r(\sum_{v=1}^{ns+1} \lambda_v x_v) = 0 \quad \text{for } r = 1,...,ne$$

$$g_m(\sum_{v=1}^{ns+1} \lambda_v x_v) \leq 0 \quad \text{for } m = 1,...,ni \qquad (1\text{-}30)$$

$$\sum_{v=1}^{ns+1} \lambda_v = 1$$

$$\lambda_v \geq 0 \quad \text{for } v = 1,...,ns+1$$

At most, two adjacent λ_v's are positive

where x_v's are the values of x at the $ns+1$ breakpoints of the piecewise linear objective

function $f(x)$. In (1-30), $h_r(x)$'s and $g_m(x)$'s are not linearized because linearity and separability is not a requirement when NLP methods are used to solve the problem. As before, when $f(x)$ is strictly convex, i.e. the problem of interest is a Category-1 problem, the adjacency constraint can be safely removed, and (1-30) can be solved with traditional smooth NLP algorithms.

For Category-3 and Category-4 problems whose convex objective functions consist of nonlinear pieces, the reformulation in (1-30) is not applicable. One can still apply the linearization trick to the objective functions as done in (1-29), provided that the memory and computation overhead is not a concern. Alternatively, (1-28) with a convex nonlinear piecewise objective function can be reformulated as

$$
\min \ f_1(0) + \sum_{v=1}^{ns} \left[f_v(y_v) - f_v(0) \right]
$$

$$
\text{s.t.} \ \ h_r(x) = 0 \quad \text{for } r = 1,...,ne
$$

$$
g_m(x) \le 0 \quad \text{for } m = 1,...,ni \qquad , \tag{1-31}
$$

$$
x_0 + \sum_{v=1}^{ns} y_v = x
$$

$$
0 \le y_v \le x_{v+1} - x_v \quad \text{for } v = 1,...,ns
$$

where x_v's are still the values of x at the $ns+1$ breakpoints of the piecewise objective function $f(x)$, and $f_v(y_v)$ is the shifted vth segment of the objective function and is defined by

$$
f_v(y_v) \equiv f(x_v + y_v) \tag{1-32}
$$

in the range $[x_v, x_{v+1}]$. This method has been used in several OPF studies to handle piecewise linear costs associated with real-energy productions [12, 13]. Essentially, each block of generation offer presented in Figure 1.1 is treated as the product of an independent generator and gets assigned a separate control variable in the OPF. A

given physical unit's contribution to the objective function therefore turns into the aggregate cost of several smoothly priced resources from smaller virtual units. Hereinafter, the reformulation method in (1-31) is referred as the decoupled power offer and bid (DPOB) method.

1.4.3 Constrained cost variables (CCV) method

For Class-5 problems that can be expressed in the minimax form, constrained cost variables can be introduced to turn the nonsmooth optimization problems into smooth ones [56]. This technique has been utilized to solve OPF problems in MATPOWER [57]. In CCV, each piecewise function in the objective is replaced by a helper cost variable that is constrained by several accompanying inequality constraints, one for each piece of the piecewise function. The new inequality constraints build a basin equivalent to requiring the helper variable to lie in the epigraph of the cost curve. When the new objective function is minimized, helper cost variables are pushed against their basins. Figure 1.8 illustrates the concept of CCV transformation using the piecewise cost curve shown in Figure 1.2. In this example, y_i is the helper variable that replaces the piecewise cost term related to the voltage V_i in the objective function. The four accompanying inequality constraints for y_i are

$$m_{iv}(V_i - V_{iv}) + C_{iv} - y_i \leq 0 \quad \text{for } v = 1,...,4 \ , \tag{1-33}$$

where m_{iv}'s are the slopes of the four cost curve segments, and V_{iv}'s and C_{iv}'s are the values of V_i and C_i at the first four breakpoints of the cost curve.

Like the separable programming method, the CCV method transforms a nonsmooth optimization problem into a smooth one and relies on good smooth constrained optimization techniques to solve the transformed problem. The scopes of the two methods, however, are different. The separable programming method is

44
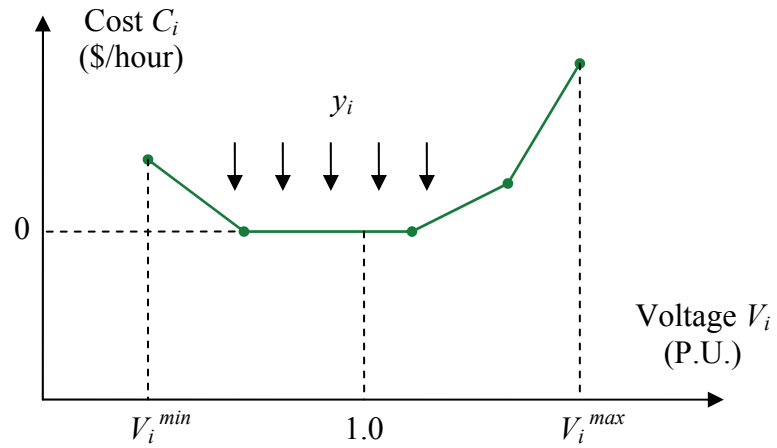
Figure 1.8 Illustration of the CCV transformation of a piecewise linear objective function using the voltage-cost example shown in Figure 1.2

applicable to Class-5 problems in Category 1, 3, and 4, while the CCV method is applicable to problems in Category1, 3, and 7. In Chapter 2, the CCV method will be extended to solve problems in Category 4, 6, and 8. When solving non-convex problems, however, global optimization techniques must be adopted as the underlying NLP methods in order to achieve globally optimal solutions.

1.5 Decomposition and parallelization

Solving the comprehensive OPF in (1-10) is a daunting task. When using NLP algorithms such as the trust-region based augmented Lagrangian method and the primal-dual interior point method, the computational complexity mainly comes from the factorization of Hessian matrices in the form of

$$
J \equiv \begin{bmatrix}
A_0 & B_1 & 0 & 0 & 0 & 0 \\
B_1{}^T & A_1 & B_2 & 0 & 0 & 0 \\
0 & B_2{}^T & A_2 & \ddots & 0 & 0 \\
0 & 0 & \ddots & \ddots & \ddots & 0 \\
0 & 0 & 0 & \ddots & A_{M-1} & B_M \\
0 & 0 & 0 & 0 & B_M{}^T & A_M
\end{bmatrix}
$$

$$
A_t \equiv \begin{bmatrix}
D_t^0 & E_t^1 & \cdots & E_t^{NC} \\
E_t^{1^T} & D_t^1 & 0 & 0 \\
\vdots & 0 & \ddots & 0 \\
E_t^{NC^T} & 0 & 0 & D_t^{NC}
\end{bmatrix} \quad \text{for } t = 0,1,...,M ,
\tag{1-34}
$$

$$
B_t \equiv \begin{bmatrix}
K_t & 0 & \ldots & 0 \\
0 & 0 & \cdots & 0 \\
\vdots & \vdots & \cdots & \vdots \\
0 & 0 & \cdots & 0
\end{bmatrix} \quad \text{for } t = 1,...,M
$$

where J is the Hessian matrix to be factorized. In (1-34), each diagonal block D is evaluated with respect to variables representing system states for a single time period

46

and a single base or contingency case. The off-diagonal blocks, E's, arise due to the contingency-couplings in (1-10), while K's come from the time-couplings. The exact structures of D's, E's, and K's depend on the underlying NLP algorithm used, and will be reviewed in later chapters when the complexity of each algorithm is analyzed. For now, it suffices to know that the size of J is $(M+1) \times (NC+1)$ times that of the Hessian matrix of a base-case single-period OPF. Due to the presence of off-diagonal elements, direct factorizations of J are impractical both in terms of computation time and in terms of memory requirements. As a result, one must seek techniques that can decompose and parallelize the task of solving (1-10) into smaller and more manageable sub-problems.

1.5.1 Benders decomposition

Benders decomposition [58] is a technique that has been frequently used in the solution of unit commitment and security-constrained OPF problems [3, 5, 14, 21, 23, 31-34]. In dealing with SCOPF, the base case (master problem) is first optimized, after which contingency analysis and re-dispatches are performed for each N-1 contingency case. In case of running into infeasibility, linear inequality constraints known as Benders cuts are added to the base-case problem to represent the level of infeasibilities of the N-1 cases. The master problem is then resolved. This procedure repeats until the master problem is solved with all N-1 cases becoming secure. Results of using this decomposition technique have been mixed. Linearization errors and possible cyclic introduction of contingency violations necessitate large number of iterations, especially for AC OPF problems. In [34], a heuristic method is proposed to reduce the number of iterations; but the results reported in the same paper show that convergence is still not a guarantee and the heuristic method may generate dispatches that are different from the expected ones. The presence of time-couplings further complicates

the application of the Benders decomposition technique to the solution of (1-10). Unlike the hub-and-spoke contingency-couplings formed among pre-contingency system states and their post-contingency counterparts, the time-couplings among system states for different time periods form a long serial chain of dependencies that dictates more nested levels of Benders decompositions, making convergence even harder to achieve.

1.5.2 Auxiliary problem principle

The auxiliary problem principle (APP) was by and large developed by Cohen as a technique that allows one to find the solution of a complex optimization problem by solving a sequence of simpler auxiliary problems [41]. It is particularly useful for decomposing large-scale non-separable problems into smaller and more manageable ones. Consider an optimization problem of the form

$$
\min \; f(X_1,...,X_N) \equiv \sum_{i=1}^{N} f_i(X_i)
$$
$$
\text{s.t.} \;\; \Theta(X_1,...,X_N) \equiv \sum_{i=1}^{N} \Theta_i(X_i) = 0
$$
. (1-35)

The solution of (1-35) through the augmented Lagrangian methods involves creating non-separable quadratic penalty terms, and is therefore not decomposable. It is shown in [24, 41] that solving (1-35) is equivalent to solving a sequence of auxiliary problems in the form of

$$
X_i^{k+1} = \arg\min \; f_i(X_i) + \frac{\beta}{2} \| X_i - X_i^k \|^2 + (\lambda_i^k)^T \Theta_i(X_i) + \gamma \, \Theta(X^k)^T \Theta_i(X_i)
$$

$$
\text{for i} = 1,...,N
$$
, (1-36)

$$
\lambda^{k+1} = \lambda^k + \gamma \, \Theta(X^{k+1})
$$

where k is the iteration number, and β and γ are constant parameters that satisfy $\beta \geq 2\gamma$. In (1-36), each sub-problem concerns only a single subset of variables and can be solved using a good NLP algorithm of choice. Convergence is achieved if X and λ's iteration-to-iteration changes are smaller than a pre-determined tolerance and equality constraints among X are satisfied.

The above APP technique has been successfully applied to the solution of OPF and unit commitment problems in several published studies [5, 18, 19, 22, 24, 26-30]. Carpentier and Bornard in [5] and Murillo-Sánchez and Thomas in [18, 22] use APP to temporally decompose unit commitment and OPF problems. For a problem in the form of

$$\min\{f_1(X) + f_2(X) \mid s(X) \in S, d(X) \in D\}, \tag{1-37}$$

where $s(X) \in S$ represents pre-contingency constraints and/or constraints for the time period T, and $d(X) \in D$ represents post-contingency constraints and/or constraints for the time period $T+1$, they first convert it to

$$\min\{f_1(X) + f_2(Y) \mid s(X) \in S, d(Y) \in D, Y - X = 0\} \tag{1-38}$$

through variable duplications, and then apply the APP technique to solve the problem by treating $Y - X$ as the Θ in (1-35). Kim and Baldick in [19, 24] and Chen, Thorp, and Mount in [29, 30] took a different path by spatially decomposing large-scale OPF's into multiple smaller regional ones. In their experiments, the system is first partitioned into several smaller regional ones linked by tie lines; dummy buses are created around those tie lines in order to separate the OPF into independent pieces, with fictitious variables and equality constraints linking them together; APP is then invoked to decouple the fictitious equality constraints and turn the problem into a sequence of multiple small-scale OPF problems.

The two APP decomposition methods mentioned above are not very effective in

solving the problem in (1-10). First, the success of the spatial decomposition technique largely depends on the granularity of the partition. Coarse partition tends to be more APP-friendly, but does not significantly remedy the matrix factorization problem associated with off-diagonal blocks in (1-34). Fine-grain partition, on the other hand, greatly reduces the sizes of those off-diagonal matrix blocks and the factorization complexity, but hurts the convergence of the APP because it involves too many tie lines and dummy constraints. Second, the temporal decomposition does not address the issue of handling inequality constraints, and is therefore not suitable for the solution of (1-10).

1.5.3 Decomposition at the matrix computation level

Given the Hessian matrix in (1-34), it is tempting for one to seek ways of decomposing the task of factorization by exploiting the structure of the matrix. One way of doing so is to reorganize J into a blocked diagonal bordered (BDB) form and parallelize the factorization block-wise. As pointed out in [13], however, the border blocks become dense during the factorization. The size of each dense sub-matrix is proportional to the number of generators in the system. Therefore, it remains prohibitedly expensive to solve (1-10) using decomposed blocked factorizations. An alternative approach is proposed in [13]. Since some NLP algorithms like the PDIPM described in 1.3.3 only require the solution of linear systems in their iterative steps, as opposed to matrix factorizations, one can use iterative methods like GMRES to replace the direct methods that involve matrix factorizations. Although good results have been reported, one should note that the success of an iterative method often hinges on the quality of its preconditioning procedures. The pre-conditioner adopted in [13] relies on proximities among pre-contingency system states and post-contingency system states. Such relations are unlikely to exist among system states of different

time periods, or among system states coupled by severe contingencies like generator outages. In addition, due to its exclusion of matrix factorizations, the method discussed in [13] does not allow one to validate the second-order KKT condition by checking the definiteness of the Hessian matrix.

1.6 Contributions of this work

This work analyzes the computational challenges of solving real-time market-based OPF's. It demonstrates, for the first time, the need for a comprehensive multi-period security-constrained OPF in the operation of real-time electricity markets. The nonsmoothness of offer/bid-driven market-based OPF's is emphasized in the study. Three techniques, namely, a trust-region based augmented Lagrangian method (TRALM), a step-controlled primal-dual interior point method (SC-PDIPM), and a modified constrained cost variables (MCCV) method, are proposed for reliable and efficient computation of large-scale nonsmooth market-based OPF's. In order to reduce the computational complexity of solving the multi-period SCOPF problem, two new decomposition techniques are proposed. In the first one, the APP decomposition method is modified to handle inequality constraints created from generator ramping limits. In the second one, binding time-coupling and contingency-coupling constraints are estimated, ranked, and filtered, before the OPF computation is decomposed and parallelized using standard block matrix computation techniques.

Chapter 2

Nonsmooth optimization for market-based optimal power flow

This chapter concerns the solution of market-base optimal OPF problems through the use of nonsmooth optimization techniques. Three separate techniques, namely, a trust-region based augmented Lagrangian method (TRALM), a step-controlled primal-dual interior point method (SC-PDIPM), and a modified constrained cost variables (MCCV) method, are proposed for reliable and efficient computation of large-scale nonsmooth market-based OPF's. TRALM integrates the augmented Lagrangian method and the trust-region unconstrained optimization technique to achieve algorithm robustness. SC-PDIPM amends the primal-dual interior point method with a step-control procedure to enhance the convergence of market-based OPF computation. The MCCV method is an extension of the CCV method introduced in Chapter 1 that handles both minimax and non-minimax problems.

2.1 Trust-region based augmented Lagrangian method

As pointed out in Chapter 1, market-based OPF's are often formulated with nonsmooth objective functions that are derived from discrete market offers and bids. For example, assuming that only piecewise linear real-energy cost is considered, the objective function of a market-based OPF takes the form of

$$C(P) = \sum_{j=1}^{NG} \{ r_j^{m'_j}(P_j - d_j^{m'_j-1}) + \sum_{m_j}[r_j^{m_j}(d_j^{m_j} - d_j^{m_j-1})]\}$$

$$m_j \in \{t \mid 1 \le t \le NS_j, \ d_j^t < P_j\} \qquad\qquad , \qquad (2\text{-}1)$$

$$m'_j \in \{t \mid 1 \le t \le NS_j, \ d_j^{t-1} < P_j < d_j^t\}$$

where r's represent the underlying offer prices, i.e. the slopes of the cost curves, d's are the real-power outputs at various breakpoints on the piecewise cost curves ($d_0 \equiv 0$), and each NS represents the number of linear pieces contained in a given piecewise linear cost curve. Costs for reactive energy, voltage support, and other more complex resources and services can take similar forms. In order to solve such nonsmooth market-based OPF's using second-order NLP algorithms, one must first convert the nonsmooth problems into smooth ones. One way of doing so is to smooth these piecewise objective functions in the regions around their breakpoints so that they become differentiable. For example, the nonsmooth objective function in (2-1) can be approximated by trigonometric functions as

$$C(P) = \sum_{j=1}^{NG} \int_0^{P_j} r'_j(x)\, dx$$

$$r'_j(d_j) = \begin{cases} r_{j_+}^{m_j} - r_{j_-}^{m_j}\cos[\pi(d_j - d_{j_-}^{m_j})/(d_{j_+}^{m_j} - d_{j_-}^{m_j})], \\ \qquad\qquad \text{if } \exists m \text{ s.t. } d_{j_-}^{m_j} < d_j < d_{j_+}^{m_j} \\ r_j(d_j), \qquad\qquad\qquad \text{otherwise} \end{cases}$$

$$r_{j_\pm}^{m_j} \equiv \frac{1}{2}(r_j^{m_j+1} \pm r_j^{m_j}) \qquad\qquad , \qquad (2\text{-}2)$$

$$d_{j_\pm}^{m_j} \equiv d_j^{m_j} - \alpha(d_j^{m_j} - d_j^{m_j\pm1})$$

$$m_j \in [1, NS_j)$$

where α is a small positive constant that controls the precision of the approximation. Figure 2.1 illustrates how the smoothing is done on a price-power curve.
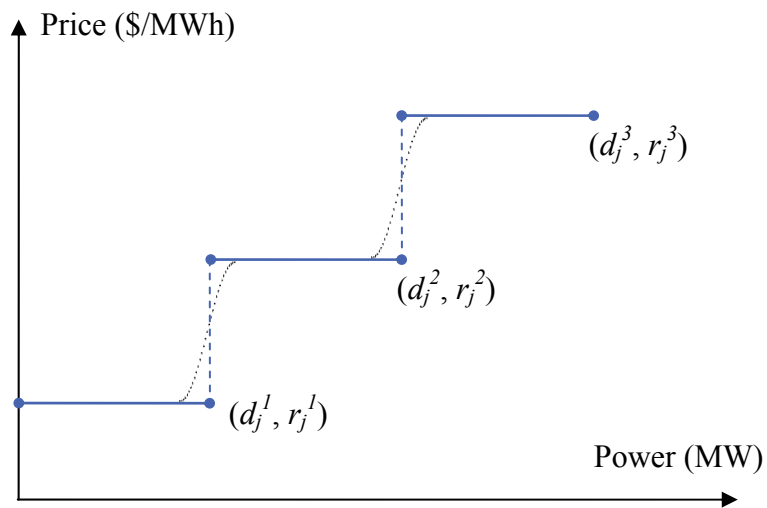
Figure 2.1 Trigonometric smoothing of a 3-segment price-power curve

Once the objective function is smoothed, one can treat the OPF problem as a smooth constrained optimization problem and apply the augmented Lagrangian method together with the trust-region method to solve it. Unlike the Newton's method, the trust-region method can handle abrupt changes of Hessian derivatives (shown by the price "jumps" in Figure 2.1) through its trust-region sizing procedures, and therefore assures global convergence. The combined trust-region based augmented Lagrangian algorithm is shown in Algorithm 2.1.

2.1.1 Complexity of TRALM

The complexity of TRALM, in the context of solving the comprehensive market-based OPF problem formulated in (1-10), is a function of the system size (*NB*, *NG*, *NL*), the system topology, offer/bid granularities (*NS*'), and cost curves smoothing accuracies (*α*'s). The look-ahead window size (*M*) and the number of contingencies (*NC*) are considered constants. For simplicity, let us assume that all cost curves have the same *NS* and *α*, and buses and generators are evenly spread across the network. Then, the overall complexity can be expressed as

$$COMP_{COPF-TRALM}(NB,NG,NL,NS,\alpha) = NI_{ALM} \times NI_{TRS} \times$$
$$NI_{TRM}(NB,NG,NL,NS,\alpha) \times \quad , \qquad (2\text{-}3)$$
$$COMP_{COPF-TRALM-FACT}(NB,NG,NL,NS,\alpha)$$

where NI_{ALM} is the number of iterations taken to solve the constrained optimization problem using Algorithm 2.1, NI_{TRM} is the number of iterations taken to solve each underlying unconstrained optimization problem using Algorithm 1.1, NI_{TRS} is the number of matrix factorizations involved in the computation of one single trust-region step (1-20), and $COMP_{COPF-TRALM-FACT}$ is the complexity of factorizing the damped Hessian matrix in (1-20). NI_{ALM} and NI_{TRS} are insensitive to system size and therefore

Algorithm 2.1

1. *Smooth the objective function of the market-based OPF according to the trigonometric smoothing technique demonstrated in (2-1) and (2-2);*

2. $k \leftarrow 0$ *; Initialize the primal variables, dual variables, penalty parameters, and tolerance parameters that are used in (1-13), (1-14), and (1-15);*

3. **while** *the convergence criteria in (1-15) is not met* **do**

   a. *Form the unconstrained optimization problem in (1-13) with the latest trial variables and parameters for iteration k;*

   b. *Solve (1-13) with the trust-region method shown in* **Algorithm 1.1***, using the direct method for matrix factorizations;*

   c. *Update the primal variables for iteration k+1 using the solution gained from 3.b*

   d. *Update the dual variables and penalty parameters for iteration k+1 according to (1-14);*

   e. *With $0 < \pi < 1$, update the gradient tolerance parameter ε^k in (1-15) according to $\varepsilon^{k+1} \leftarrow \max(\pi\varepsilon^k, \varepsilon^\infty)$;*

   f. $k \leftarrow k+1$

   end do

treated as constants. $NI_{TRM}(NB, NG, NL, NS, \alpha)$ can be empirically derived through numerical experiments and will be shown in later sections. To estimate $COMP_{COPF-TRALM-FACT}(NB, NG, NL, NS, \alpha)$, recall the structure of the Hessian matrix J in (1-34). For TRALM, D_t^{ci} in (1-34) is a ($2NB+2NG$) by ($2NB+2NG$) sparse matrix that represents the diagonal block of the Hessian matrix corresponding to the set of variables (P_t^{ci}, Q_t^{ci}, V_t^{ci}, θ_t^{ci}) for the time period t and the contingency case ci ($ci = 0$ is for the base case); E_t^{ci} and K_t are sparse matrices of the same size, but with non-zero entries (two per row/column) only in the (P_t^{ci}, P_t^{ci}) portion, representing generator ramping limits. The damped Hessian matrix in (1-20) has the same structure as that of J, which is independent of NS and α. Therefore, the factorization complexity for the solution of (1-20) degenerates into $COMP_{COPF-TRALM-FACT}(NB, NG, NL)$. Due to the presence of E_t^{ci}'s and K_t's, matrix fill-ins created in a direct factorization of the damped Hessian matrix will at least amount to a dense NG by NG matrix. As a result, the factorization complexity for the comprehensive OPF problem can be expressed as

$$COMP_{COPF-TRALM-FACT}(NB, NG, NL) = O(NB) + O(NL) + O(NG^3). \qquad (2\text{-}4)$$

The overall complexity of solving (1-10) using TRALM is

$$COMP_{COPF-TRALM}(NB, NG, NL, NS, \alpha) = NI_{ALM} \times NI_{TRS} \times$$
$$NI_{TRM}(NB, NG, NL, NS, \alpha) \times \qquad . \qquad (2\text{-}5)$$
$$[O(NB) + O(NL) + O(NG^3)]$$

For systems with large numbers (hundreds or even thousands) of generators, the complexity in (2-5) is clearly unacceptable for real-time applications. In Chapter 3, algorithms will be introduced to decompose the comprehensive OPF into multiple single-period base-case OPF's. In that case, with a good preconditioned factorization algorithm such as the one used in UFSparse, the complexity of the factorization

becomes linear, i.e.

$$COMP_{OPF-TRALM-FACT}(NB, NG, NL) = O(NB) + O(NL) + O(NG). \qquad (2\text{-}6)$$

The overall complexity of TRALM applied to the single-period base-case OPF is therefore

$$COMP_{OPF-TRALM}(NB, NG, NL, NS, \alpha) = NI_{ALM} \times NI_{TRS} \times$$

$$NI_{TRM}(NB, NG, NL, NS, \alpha) \times \qquad (2\text{-}7)$$

$$[O(NB) + O(NL) + O(NG)]$$

2.2 Step-controlled primal-dual interior point method

To apply the primal-dual interior point method to the solution of (1-10), one first needs to carry out the same cost-curve smoothing procedure as illustrated in (2-2) and Figure 2.1. Since the PDIPM method introduced in Chapter 1 is not a global convergent algorithm, one cannot apply it directly to the smoothed problem, whose objective function is still subject to abrupt derivative changes. As shown in the 118-bus OPF example in Figure 2.2, the gradient and Hessian variables used in (1-23) and (1-24) change drastically from iteration to iteration when dealing with the market-based OPF, destroying the strong descending property of Newton steps.

In order to overcome the above difficulty, we can introduce a step control procedure in the PDIPM algorithm to prevent bold Newton steps from destroying the descending property. At each PDIPM iteration, the Newton step is first computed as described in Chapter 1, and then shortened recursively until the quadratic approximation of the Lagrangian along the shortened step is close to the actual Lagrangian. Empirically, it is more efficient to start applying such step control procedure after the normal PDIPM step fails to improve the gradient condition or the
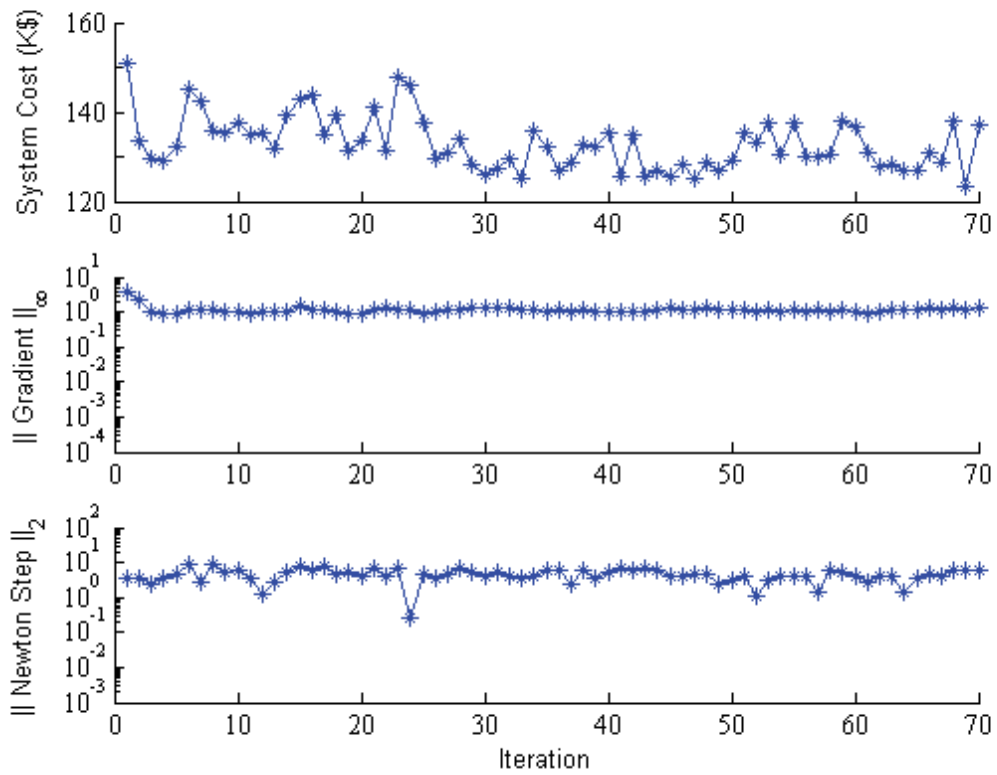
Figure 2.2 Progression of PDIPM iterations in solving a single-period 118-bus market-based OPF problem ($NS = 3$, $\alpha = 0.01$)

feasibility condition. The whole step-controlled primal-dual interior point method (SC-PDIPM) is shown in Algorithm 2.2. Although it uses PDIPM as the baseline algorithm, the same step control concept applies to other interior point methods as well. As shown in Figure 2.3, with step adjustments, SC-PDIPM is now able to reduce both system cost and gradients continuously along the progression of iterations.

2.2.1 Complexity of SC-PDIPM

Like that of TRALM, the complexity of SC-PDIPM in the solution of the comprehensive market-based OPF problem in (1-10) can be expressed as

$$COMP_{COPF-SCPDIPM}(NB, NG, NL, NS, \alpha) = NI_{SCPDIPM}(NB, NG, NL, NS, \alpha) \times$$
$$COMP_{COPF-SCPDIPM-FACT}(NB, NG, NL) \qquad (2\text{-}8)$$

where $NI_{SCPDIPM}$ is the number of major iterations taken in Algorithm 2.2 and $COMP_{COPF-SCPDIPM-FACT}$ is the complexity of the matrix factorization in (1-24). The computational effort of the inner loop of Algorithm 2.2 is negligible. Again, recall the structure of the Hessian matrix J in (1-34), D_t^{ci} is a (4NB+2NG) by (4NB+2NG) sparse matrix that corresponds to (P_t^{ci}, Q_t^{ci}, V_t^{ci}, θ_t^{ci}, λ_t^{ci}) in this case, while E_t^{ci} and K_t still only have non-zero entries (two per row/column) representing generator ramping limits in the (P_t^{ci}, P_t^{ci}) portion. Similarly, without any decomposition, $COMP_{COPF-SCPDIPM-FACT}$ is

$$COMP_{COPF-SCPDIPM-FACT}(NB, NG, NL) = O(NB) + O(NL) + O(NG^3), \qquad (2\text{-}9)$$

while the matrix factorization complexity for the single-period base-case OPF is

$$COMP_{OPF-SCPDIPM-FACT}(NB, NG, NL) = O(NB) + O(NL) + O(NG). \qquad (2\text{-}10)$$

Although the size of the Hessian matrix used in SC-PDIPM is larger than that in TRALM, the underlying constants implied in (2-9) and (2-10) are not significantly

Algorithm 2.2

Let $0 < \kappa < 1, 0 < \eta << 1, 0 < \varepsilon << 1, X_0, Z_0, \lambda_0, \mu_0,$ and γ_0 be given,

$scipm \leftarrow false; \quad L_t \equiv L^{\gamma_t}(X_t, Z_t, \lambda_t, \mu_t);$

$\psi_t(\Delta X_t) \equiv (\nabla_X L_t)^T \Delta X_t + \frac{1}{2}(\Delta X_t)^T (\nabla_X^2 L_t) \Delta X_t$

$\rho_t(\Delta X_t) \equiv \dfrac{L^{\gamma_t}(X_t + \Delta X_t, Z_t, \lambda_t, \mu_t) - L_t}{\psi_t(\Delta X_t)}$

$fcond_t \equiv \dfrac{\max(\max\limits_{1 \leq j \leq ni}[G_j(X_t)], \| H(X_t) \|_\infty)}{1 + \max(\| \lambda_t \|_\infty, \| \mu_t \|_\infty)};$

$gcond_t \equiv \dfrac{\| \nabla_X L_t \|_\infty}{1 + \max(\| \lambda_t \|_\infty, \| \mu_t \|_\infty)}$

$ccond_t \equiv \dfrac{\mu_t^T Z_t}{1 + \| X_t \|_\infty}; \quad ocond_t \equiv \dfrac{\| f(X_t) - f(X_{t-1}) \|}{1 + \| f(X_{t-1}) \|}$

while $\forall cond \in (fcond_t, gcond_t, ccond_t, ocond_t) > \varepsilon$ **do**

    compute $(\Delta X_t, \Delta Z_t, \Delta\lambda_t, \Delta\mu_t)$ according to $(1-24)$

    if $scipm = true$

        while $\rho_t(\Delta X_t) < 1 - \eta$ **or** $\rho_t(\Delta X_t) > 1 + \eta$ **do**

            $\Delta X_t \leftarrow \kappa \Delta X_t; \; \Delta Z_t \leftarrow \kappa \Delta Z_t; \; \Delta\lambda_t \leftarrow \kappa \Delta\lambda_t; \; \Delta\mu_t \leftarrow \kappa \Delta\mu_t;$

        end do

    end if

    compute $(X_{t+1}, Z_{t+1}, \lambda_{t+1}, \mu_{t+1}, \gamma_{t+1})$ according to $(1-25)$ and $(1-26)$

    if $fcond_{t+1} \geq fcond_t$ **and** $gcond_{t+1} \geq gcond_t$

        $scipm \leftarrow true$

    end if

    $t \leftarrow t + 1$

end do
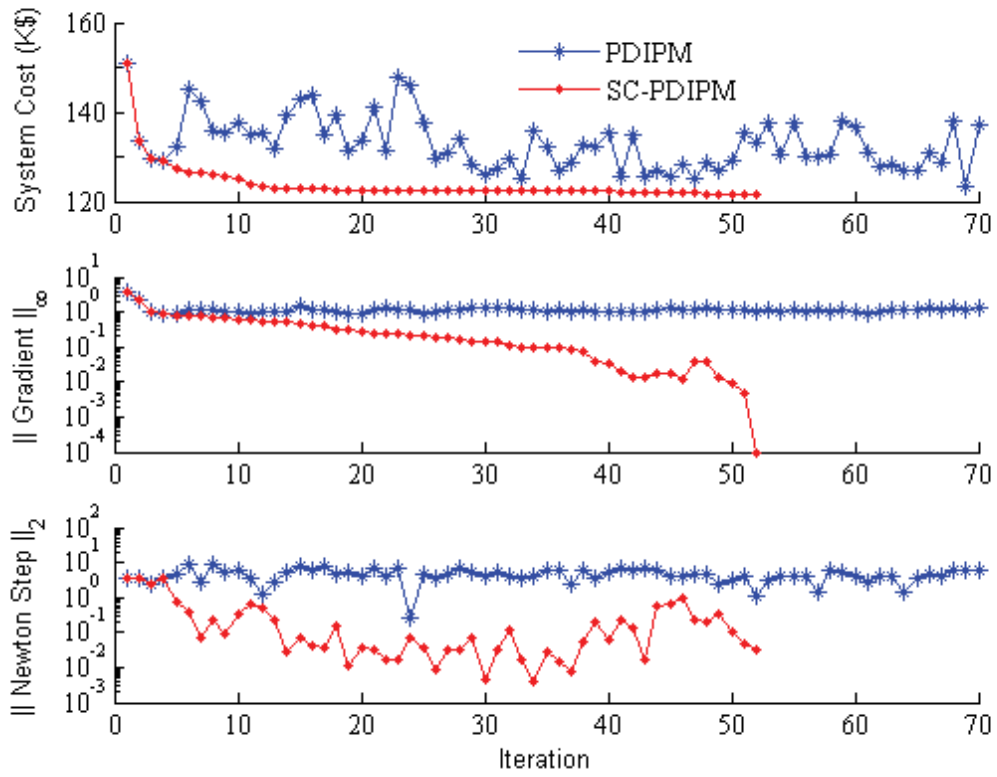
Figure 2.3 A comparison of PDIPM and SC-PDIPM in solving the single-period 118-bus market-based OPF problem (*NS* = 3, *α* = 0.01)

different from those in (2-4) and (2-6), because the numbers of non-zero entries are essentially the same in the two cases. The overall complexity of SC-PDIPM for solving the comprehensive OPF is

$$COMP_{COPF-SCPDIPM}(NB, NG, NL, NS, \alpha) = NI_{SCPDIPM}(NB, NG, NL, NS, \alpha) \times$$
$$[O(NB) + O(NL) + O(NG^3)] \quad , (2\text{-}11)$$

where $NI_{SCPDIPM}$ will be empirically derived from numerical experiments later. And the complexity of solving the single-period base-case OPF is

$$COMP_{OPF-SCPDIPM}(NB, NG, NL, NS, \alpha) = NI_{SCPDIPM}(NB, NG, NL, NS, \alpha) \times$$
$$[O(NB) + O(NL) + O(NG)] \quad . (2\text{-}12)$$

2.3 Modified constrained cost variables method (MCCV)

The CCV formulation introduced in Chapter 1 is an effective way of turning Category 1, 3, and 7 nonsmooth optimization problems into smooth ones. An extension to CCV is proposed here to make it also applicable to problems in Category 4, 6, and 8. Let us consider two adjacent finite segments of a piecewise objective function $f(x)$ and the underlying functions $fl(x)$ and $fr(x)$ representing them shown in Figure 2.4. Assume that the two endpoints of the left segment $fl(x)$ are a and b, and the two endpoints of the right segment $fr(x)$ are b and c. In Figure 2.4, the solid line representing $f(x)$ falls below $fl(x)$ in part of the [b, c] range, and thus cannot be uniformly expressed as the maximum of its member functions $fl(x)$ and $fr(x)$ in [a, c]. In order to use the CCV reformulation technique, one can define new member functions $fl'(x)$ and $fr'(x)$ as

$$fl'(x) = \begin{cases} fl(b) + \int_b^x rl'(x) \, dx, & \text{if } x > b \\ fl(x), & \text{if } x \leq b \end{cases} \quad (2\text{-}13)$$
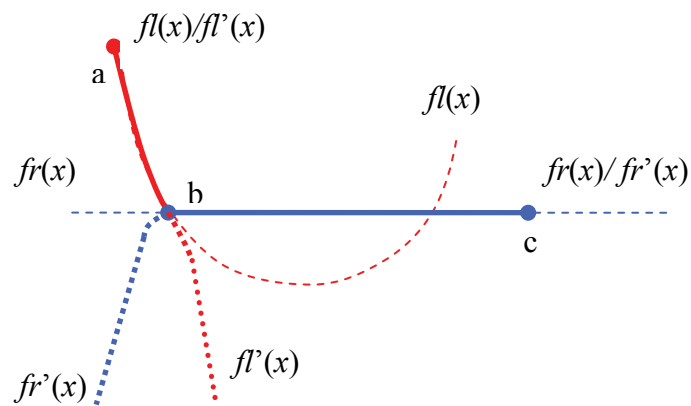
Figure 2.4 Illustration of the function extension procedure of MCCV: $fl'(x)$ and $fr'(x)$ replace $fl(x)$ and $fr(x)$ in regions beyond the breakpoint b to the right and to the left, respectively; the objective function $f(x)$, represented by the solid line, can be expressed as the maximum of $fl'(x)$ and $fr'(x)$ in [a, c]; The original optimization problem is turned into a minimax problem once the function extension procedure is done on all member functions and breakpoints of $f(x)$.

$$fr'(x) = \begin{cases} fr(b) + \int_b^x rr'(x)\,dx, & \text{if } x < b \\ fr(x), & \text{if } x \geq b \end{cases}$$

$$rl'(x) = \begin{cases} rl_+ - rl_- \cos[\pi(x-b)/(xl_+ - b)], & \text{if } b < x < xl_+ \\ rmin, & \text{if } x \geq xl_+ \end{cases}$$

$$rr'(x) = \begin{cases} rr_+ - rr_- \cos[\pi(x-b)/(xr_- - b)], & \text{if } xr_- < x < b \\ rmax, & \text{if } x \leq xr_- \end{cases}$$

$$rl \equiv \nabla fl; \qquad rr \equiv \nabla fr \qquad\qquad , \qquad (2\text{-}13)$$

$$rmin \equiv \min(\nabla f(x)); \qquad rmax \equiv \max(\nabla f(x))$$

$$rl_\pm \equiv \frac{1}{2}(rmin \pm rl(b)); \qquad rr_\pm \equiv \frac{1}{2}(rmax \pm rr(b))$$

$$xl_+ \equiv b + \alpha(c - b); \qquad xr_- \equiv b + \alpha(a - b)$$

to replace the member functions $fl(x)$ and $fr(x)$ in the objective function. The two extended functions fall below the desired CCV epigraph in regions beyond the breakpoint b to the right and to the left, respectively. Once this procedure is carried out for all segments and breakpoints of the piecewise objective function $f(x)$, one can rewrite the objective function as the maximum of all its extended member functions, reformulate the minimax optimization problem using the CCV reformulation technique introduced in Chapter 1. Algorithm 2.3 outlines the modified CCV method together with PDIPM as the underlying NLP solver. Note that for non-convex problems that fall into Category 6 and 8 listed in Table 1.1, in order to achieve the global optimum, the proposed MCCV method must be used in conjunction with global optimization techniques, which are out of the scope of this work.

2.3.1 Complexity of MCCV

The complexity of MCCV, with PDIPM as the underlying NLP solver, is

Algorithm 2.3

Apply $(2-13)$ to all neighbor segments of the piecewise objective function

Reformulate the problem into a smooth one in the form of $(1-11)$ using CCV

Let $0 < \varepsilon << 1, X_0, Z_0, \lambda_0, \mu_0$, and γ_0 be given,

$$L_t \equiv L^{\gamma_t}(X_t, Z_t, \lambda_t, \mu_t);$$

$$fcond_t \equiv \frac{\max(\max_{1 \le j \le ni}[G_j(X_t)], \|H(X_t)\|_\infty)}{1 + \max(\|\lambda_t\|_\infty, \|\mu_t\|_\infty)};$$

$$gcond_t \equiv \frac{\|\nabla_X L_t\|_\infty}{1 + \max(\|\lambda_t\|_\infty, \|\mu_t\|_\infty)}$$

$$ccond_t \equiv \frac{\mu_t^T Z_t}{1 + \|X_t\|_\infty}; \quad ocond_t \equiv \frac{\|f(X_t) - f(X_{t-1})\|}{1 + \|f(X_{t-1})\|}$$

while $\forall cond \in (fcond_t, gcond_t, ccond_t, ocond_t) > \varepsilon$ **do**

    compute $(\Delta X_t, \Delta Z_t, \Delta \lambda_t, \Delta \mu_t)$ according to $(1-24)$

    compute $(X_{t+1}, Z_{t+1}, \lambda_{t+1}, \mu_{t+1}, \gamma_{t+1})$ according to $(1-25)$ and $(1-26)$

    $t \leftarrow t + 1$

end do

$$COMP_{COPF-MCCV}(NB, NG, NL, NS) = NI_{MCCV}(NB, NG, NL, NS) \times$$
$$COMP_{COPF-MCCV-FACT}(NB, NG, NL, NS) \qquad (2\text{-}14)$$

where NI_{MCCV} is the number of PDIPM iterations taken. Similar to the factorization complexity of SC-PDIPM, the complexity of a Hessian matrix factorization involved in MCCV is

$$COMP_{COPF-MCCV-FACT}(NB, NG, NL, NS) = O(NB) + O(NL) + O(NG^3)$$
$$+ O(NS) \qquad (2\text{-}15)$$

for the multi-period security-constrained OPF problem in (1-10), and the overall complexity of solving (1-10) without using decomposition techniques is

$$COMP_{COPF-MCCV}(NB, NG, NL, NS) = NI_{MCCV}(NB, NG, NL, NS) \times$$
$$[O(NB) + O(NL) + O(NG^3) + O(NS)] \qquad (2\text{-}16)$$

If decomposition techniques are used, the complexity of factorizing the Hessian matrix for a single-period base-case OPF is

$$COMP_{OPF-MCCV-FACT}(NB, NG, NL, NS) = O(NB) + O(NL) + O(NG)$$
$$+ O(NS) \qquad (2\text{-}17)$$

and the overall complexity of solving the single-period base-case OPF is

$$COMP_{OPF-MCCV}(NB, NG, NL, NS) = NI_{MCCV}(NB, NG, NL, NS) \times$$
$$[O(NB) + O(NL) + O(NG) + O(NS)] \qquad (2\text{-}18)$$

In the above analysis, the number of individual cost curves included in the objective function is assumed to be on the order of $O(NB)+O(NG)+O(NL)$. The extra linear term $O(NS)$ arises from the non-zero elements of $\nabla G(X)[\mu/Z]\nabla G(X)^T$ in (1-24), which are created due to the presence of extra inequality constraints accompanying constrained cost variables. Note that this extra term would be $O(NS^3)$ for the separable

programming and DPOB methods introduced in Chapter 1.

2.4 Numerical results

The new OPF algorithms and the MCCV reformulation method have been tested and compared with some existing OPF techniques using the power system models listed in Table 2.1 (See Appendix A for details). Tests were carrier out on a PC with Intel 3.3GHz P4 processor (2MB L2 cache), 2GB memory, and Linux 2.6.9 kernel. All optimization programs and auxiliary numerical utilities, except the LU and Cholesky factorization modules, were developed in house using Standard C and compiled using the GCC 3.4.4 compiler. LU and Cholesky factorizations were implemented using the UFsparse package [59]. The parameters used in PDIPM, TRALM, SC-PDIPM, MCCV, and cost-curve smoothing, unless stated otherwise, were set according to Table 2.2. All experiments assumed flat starting points, i.e. unit voltages, zero phase angles, and generator outputs at the midpoints between maximum generations and minimum generations. Market offers and bids were randomly generated.

2.4.1 Convergence and performance

Table 2.3 compares the convergence and performance properties of four algorithms in the solution of classical single-period base-case OPF problems. TRALM and SC-PDIPM converged in all cases, while MINOS [57, 60] failed to solve large-scale OPF's and PDIPM failed to solve OPF's with piecewise costs. SC-PDIPM is faster than TRALM and better suited for real-time applications.

One pitfall of SC-PDIPM, like that of PDIPM, is its lack of global convergence guarantee. Some variations of PDIPM can improve the convergence through the use of line searching and/or damped Newton procedures [12, 51], but only at the cost of

Table 2.1 Summary of the power system models used in the study

System	Buses	Generators	Branches	Load (MW)
1	30	6	41	189
2	57	7	80	1,250
3	118	54	186	4,242
4	300	69	411	23,525
5	2383	327	2896	24,558
6	2935	956	7028	394,794

Table 2.2 Parameters used in PDIPM, TRALM, SC-PDIPM, and MCCV

$NS = 3,\ \alpha = 0.04$							
TRALM				PDIPM/SC-PDIPM			
ε_λ	5e-3	T	0.25	κ	0.5	Z_0	1.0
ε_μ	1e-1	H	0.75	η	0.1	λ_0	0.0
ε^0	2e0	γ_1	0.1	ε	1e-5	μ_0	1.0
ε^∞	1e-2	γ_2	2.0	X_0	flat start	γ_0	1.0
$\beta_{W,\ U} = 3$		$\gamma_{W,\ U} = 0.33$		$\xi = 0.99995$		σ	0.1

Table 2.3 Comparisons of the execution time (sec.) and numbers of iterations (shown in parenthesis) of four algorithms in the solution of single-period base-case OPF's

Solving OPF's with Quadratic Costs				
System	MINOS	PDIPM	TRALM	SC-PDIPM
1	0.06 (350)	0.05 (13)	0.20 (134)	0.07 (13)
2	0.07 (179)	0.11 (14)	0.40 (146)	0.17 (17)
3	1.2 (1579)	0.37 (21)	2.3 (441)	0.57 (24)
4	6.3 (3654)	1.2 (29)	4.8 (420)	1.3 (24)
5	FAIL	12 (33)	168 (1834)	14 (33)
6	FAIL	22 (34)	680 (2842)	26 (34)
Solving OPF's with Piecewise Costs				
System	MINOS	PDIPM	TRALM	SC-PDIPM
1	0.04 (163)	0.66 (171)	0.34 (221)	0.15 (26)
2	0.07 (184)	0.93 (126)	0.40 (171)	0.47 (45)
3	0.9 (1190)	FAIL	3.7 (698)	1.9 (77)
4	3.8 (2002)	27 (689)	6.7 (544)	4.0 (72)
5	FAIL	FAIL	202 (2193)	54 (122)
6	FAIL	FAIL	1011 (4310)	161 (204)

losing performance advantage. In [12], Jabr et al. demonstrate cases in which PDIPM would fail. Experiments in this study, however, show that SC-PDIPM, as PDIPM in the context of solving OPF's with quadratic costs, consistently converges to the desired OPF solutions, with both the first-order and the second-order KKT conditions satisfied. The failure of PDIPM demonstrated in [12] might be attributed to the special OPF formulation used in [12] that treats all constraints as inequality constraints. The encouraging results reported in this study imply that the OPF problem's nonlinearity is relatively mild and its region of attraction is large enough to counter occasional ill-defined Newton steps.

Table 2.4 compares three different OPF formulations (the classical, DPOB, and MCCV) in the solution of market-based OPF's, with PDIPM or SC-PDIPM as the underlying NLP algorithm. MCCV and DPOB in conjunction with PDIPM offer better performances than the combination of the classical formulation and SC-PDIPM. Compared to DPOB, the classical formulation and MCCV have the advantages of being extendable to solving nonsmooth problems in all categories listed in Table 1.1.

2.4.2 Accuracy

Given a benchmark OPF solution

$$(C^*, P^*, Q^*, V^*, \theta^*, \lambda^*_{FA,FR}, \mu^*_{P\pm,Q\pm,V\pm,SF,ST})$$

and a solution

$$(C, P, Q, V, \theta, \lambda_{FA,FR}, \mu_{P\pm,Q\pm,V\pm,SF,ST})$$

generated by a new OPF tool under study, one can use the following metrics to verify the legitimacy of the new tool:

Table 2.4 Execution time (sec.) and numbers of iterations (shown in parenthesis) of solving differently formulated OPF's

System	OPF's with Convex Piecewise Linear Costs		
	Classical-SC-PDIPM	DPOB-PDIPM	MCCV-PDIPM
1	0.15 (26)	0.06 (13)	0.06 (15)
2	0.47 (45)	0.11 (13)	0.17 (22)
3	1.9 (77)	0.39 (19)	1.9 (109)
4	4.0 (72)	1.3 (30)	1.2 (28)
5	54 (122)	13 (35)	15 (43)
6	161 (204)	32 (47)	49 (78)

$$\delta_C \equiv \max(\, | \, C - C^* \, | / (1 + | \, C^* \, |) \,)$$

$$\delta_X \equiv \max(| \, [(P^* + e)]^{-1}(P - P^*)|_\infty, | \, [(V^* + e)]^{-1}(V - V^*)|_\infty)$$

$$\delta_\lambda \equiv \max(\, | \, [(\lambda_{FA}^* + e)]^{-1}(\lambda_{FA} - \lambda_{FA}^*)|_\infty, | \, [(\lambda_{FR}^* + e)]^{-1}(\lambda_{FR} - \lambda_{FR}^*)|_\infty)$$

$$\delta_\mu \equiv \max(\, | \, [(\mu_{P\pm}^* + e)]^{-1}(\mu_{P\pm} - \mu_{P\pm}^*)|_\infty, | \, [(\mu_{Q\pm}^* + e)]^{-1}(\mu_{Q\pm} - \mu_{Q\pm}^*)|_\infty, \qquad \text{(2-19)}$$

$$| \, [(\mu_{V\pm}^* + e)]^{-1}(\mu_{V\pm} - \mu_{V\pm}^*)|_\infty, | \, [(\mu_{SF}^* + e)]^{-1}(\mu_{SF} - \mu_{SF}^*)|_\infty,$$

$$| \, [(\mu_{ST}^* + e)]^{-1}(\mu_{ST} - \mu_{ST}^*)|_\infty)$$

Small δ's indicate good OPF solutions.

Table 2.5 lists the result of a cross examination of OPF solutions generated by MINOS, TRALM, SC-PDIPM, DPOB-PDIPM, and MCCV-PDIPM. The small values reported in Table 2.5 indicate that all methods proposed are valid for the computation of large-scale market-based OPF's.

The parameter α used in cost-curve smoothing has an impact on the accuracies of TRALM and SC-PDIPM's solutions. As shown in Table 2.6, smaller α's yield more accurate solutions. In practice, 0.04 is small enough for α to ensure satisfactory results. Since the experiments in this study only use quadratic costs and piecewise linear convex costs, the piecewise function extension procedure in (2-13) is not invoked for MCCV. Hence, MCCV's results do not vary with α.

2.4.3 Scalability

The time taken to solve an OPF problem depends on both the number of iterations taken and the computational complexity of a single iteration. Assuming a constant transmission network density and a constant fill-in ratio for the sparse matrix factorization, the complexity of a single PDIPM, TRALM, or SC-PDIPM iteration is $O(NB)$ for single-period base-case OPF problems. Although the exact relationship

TABLE 2.5 Accuracies of OPF solutions computed by different algorithms (300-bus system, MINOS as the reference)

Algorithm	δ_C	δ_X	δ_λ	δ_μ
TRALM	5.2e-4	2.6e-2	1.6e-3	9.0e-3
SC-PDIPM	5.2e-4	2.7e-2	1.6e-3	8.6e-3
DPOB-PDIPM	2.9e-7	1.3e-3	1.0e-4	3.6e-4
MCCV-PDIPM	7.1e-5	5.4e-4	5.5e-5	8.6e-5

Table 2.6 Accuracies of several OPF solutions computed by SC-PDIPM with different α values (300-bus system, MCCV-PDIPM as the reference)

α	δ_C	δ_X	δ_λ	δ_μ
0.1	1.3e-3	4.6e-2	3.6e-3	2.4e-2
0.04	5.2e-4	2.7e-2	1.6e-3	8.6e-3
0.01	1.3e-4	6.9e-3	4.1e-4	2.1e-3

between the system size and the number of iterations is unclear, one can identify some general trends from Table 2.3 and 2.4. First, the number of iterations rises as the system size increases. Second, the rising paces for PDIPM and SC-PDIPM are much slower than those of MINOS and TRALM, suggesting that SC-PDIPM and MCCV-PDIPM are more scalable and better suited for large-scale systems. Third, as indicated in (2-5), (2-7), (2-11), (2-12), (2-16), and (2-18), other system details such as the number of generators can also have impacts on the algorithm complexities. Omitting those system-specific characteristics, the overall complexity of solving single-period base-case OPF can be approximated by $O(NB^{1+\varepsilon})$, where ε is a small number that falls between 0.1 and 0.2 for SC-PDIPM and MCCV-PDIPM according to the results in Table 2.3 and 2.4.

The number of segments (*NS*) contained in piecewise cost curves also impacts the performance of second-order NLP-based OPF algorithms. Table 2.7 lists the execution time and numbers of iterations taken by SC-PDIPM, DPOB-PDIPM, and MCCV-PDIPM to solve a 2935-bus OPF with different *NS* values. The number of iterations taken by SC-PDIPM grows approximately linearly with *NS*, while those by DPOB-PDIPM and MCCV-PDIPM are insensitive to *NS*. One should note that DPOB and MCCV's scalabilities are limited to small *NS*'s. For large *NS*'s, DPOB dictates dense $\nabla H(X)$'s and is therefore unscalable both in terms of speed and in terms of memory requirement. MCCV, on the other hand, does not encounter such problem, because each accompanying constraint that it adds to the problem only contains small and fixed number of variables. Depending on the underlying computing platform used, the extra memory required by MCCV to accommodate new inequality constraints and helper cost variables may or may not be an issue. That said, one does not need to worry about DPOB and MCCV's scalabilities for today's electricity market operations, where *NS* is often capped around 10~20. In the future, however, fine-grain trading

Table 2.7 Execution time (sec.) and numbers of iterations taken to solve a single-period base-case 2935-bus OPF with different *NS* values

SC-PDIPM					
NS	# Its.	Time	*NS*	# Its.	Time
3	204	161	4	218	173
5	217	172	6	263	210
7	323	263	8	344	278
9	362	292	10	402	328

DPOB-PDIPM					
NS	# Its.	Time	*NS*	# Its.	Time
3	47	32	4	48	33
5	46	33	6	48	35
7	47	35	8	45	35
9	46	36	10	46	37

MCCV-PDIPM					
NS	# Its.	Time	*NS*	# Its.	Time
3	78	49	4	98	61
5	72	46	6	98	62
7	76	49	8	87	56
9	74	48	10	97	62

could be instituted and present significant challenge to the two alternative OPF formulations.

2.5 Remarks

In this chapter, three new techniques (TRALM, SC-PDIPM, and MCCV) are proposed to solve market-based nonsmooth OPF problems. Numerical studies show that these techniques are reliable and better than some existing ones. MCCV-PDIPM and SC-PDIPM are particularly good for real-time applications due to their efficiencies, while TRALM can be applied as a backup technique that offers global convergence guarantee. The CCV method has been extended to solve Class-5 composite nonsmooth problems in all categories discussed in Chapter 1. When dealing with non-convex costs, however, the methods discussed in this work must be combined with global optimization techniques in order to achieve global optimal solutions. Compared to the separable programming approach DPOB, MCCV offers better scalability with regards to NS because it avoids increasing the number of non-zeros per row/column in $\nabla H(X)$. In the future, one needs to pay attention to DPOB and MCCV's large memory requirements as the market embraces finer-grain electricity trading.

Chapter 3

Multi-period security-constrained optimal power flow

This chapter discusses the solution of the multi-period security-constrained OPF problem formulated in (1-10). In Chapter 1 and Chapter 2, we have seen that the main difficulty of solving the comprehensive OPF problem is the excessive computation overhead (on the order of $O(NG^3)$) associated with matrix fill-ins that are created during the factorization of Hessian matrices. Two decomposition methods are proposed in this Chapter to address the issue. In Chapter 3.1, the auxiliary problem principle method introduced in Chapter 1 is extended to treat the time-coupling and contingency-coupling inequality constraints in (1-10) and make the problem decomposable. Chapter 3.2 introduces a look-ahead OPF method that estimates the binding generator ramping constraints ahead of time and reduces the number of time-coupling and contingency-coupling constraints that go into (1-10). In both methods, the dense sub-matrices presented in the factorized Hessian matrix are either eliminated or shrunk significantly. This will allow us to adopt the algorithms in Chapter 2 to solve (1-10) without incurring much computational overhead.

3.1 Modified APP method

The APP method introduced in Chapter 1 has been applied with a limited degree of

success to the decomposition of OPF problems whose sub-problems are coupled by equality constraints [5, 18, 19, 22, 24, 26-30]. The comprehensive OPF in (1-10), however, is a collection of optimization problems that are linked by inequality (generator ramping) constraints, and therefore cannot be directly solved using the APP method in (1-35) and (1-36).

For an optimization problem in the form of

$$\min\{f_1(X) + f_2(Y) \mid s(X) \in S, \, d(Y) \in D, \, Y_M - X_M \le 0\}, \tag{3-1}$$

where X_M and Y_M are subsets of X and Y, one may tempt to first convert the coupling inequality constraints into equality ones through the introduction of new variables as

$$\min\{f_1'(X, Z_M) + f_2(Y) \mid s'(X, Z_M) \in S', \, d(Y) \in D, \, Y_M - Z_M = 0\}$$

$$\{(X, Z_M) \mid s'(X, Z_M) \in S'\} \equiv \{(X, Z_M) \mid s(X) \in S, \, Z_M - X_M \le 0\} \quad , \tag{3-2}$$

$$f_1'(X, Z_M) \equiv f_1(X)$$

and then apply the APP method in Chapter 1 to decompose the problem into a sub-problem on (X, Z_M) and a sub-problem on Y, which are coupled by the equality constraints $Y_M - Z_M = 0$ instead of inequality constraints. Unfortunately, this method fails to yield convergence when generator ramping constraints are binding. Table 3.1 and Figure 3.1 show the results of solving an example 30-bus comprehensive OPF using the stated method.

To be able to handle the inequality coupling constraints in (3-1), one can decompose the problem into the following iterative set of auxiliary problems:

$$X^{k+1} = \arg\min_{s(X) \in S} f_1(X) + \sum_{i=1}^{NCI} \begin{cases} \dfrac{\beta^k}{2}(X_{m_i} - X_{m_i}^k)^2 + \gamma^k (Y_{m_i}^k - X_{m_i}^k)(Y_{m_i}^k - X_{m_i}) \\[2mm] \quad - \mu_{m_i}^k X_{m_i}, \quad \text{if } \mu_{m_i}^k + \gamma^k(Y_{m_i}^k - X_{m_i}^k) > 0 \\[4mm] 0, \quad\quad\quad\quad\quad \text{if } \mu_{m_i}^k + \gamma^k(Y_{m_i}^k - X_{m_i}^k) \le 0 \end{cases} \tag{3-3}$$

Table 3.1 Results of solving 30-bus multi-period market-based OPF's using the classic

APP method ($M = 2$, $T_R = 20$ minutes, $t_0 \rightarrow$ 8:00PM). No contingency is considered.

Time Period	Number of Binding Ramping Limits	Number of APP Iterations
$RA = 1\%$ of generator capacity per minute		
t_0	0	5
$t_0 + 1$	1	FAIL
$RA = 2\%$ of generator capacity per minute		
t_0	0	5
$t_0 + 1$	0	6
$t_0 + 2$	0	6
$t_0 + 3$	0	5
$t_0 + 4$	0	7
$t_0 + 5$	0	7
$t_0 + 6$	0	5
$t_0 + 7$	2	FAIL
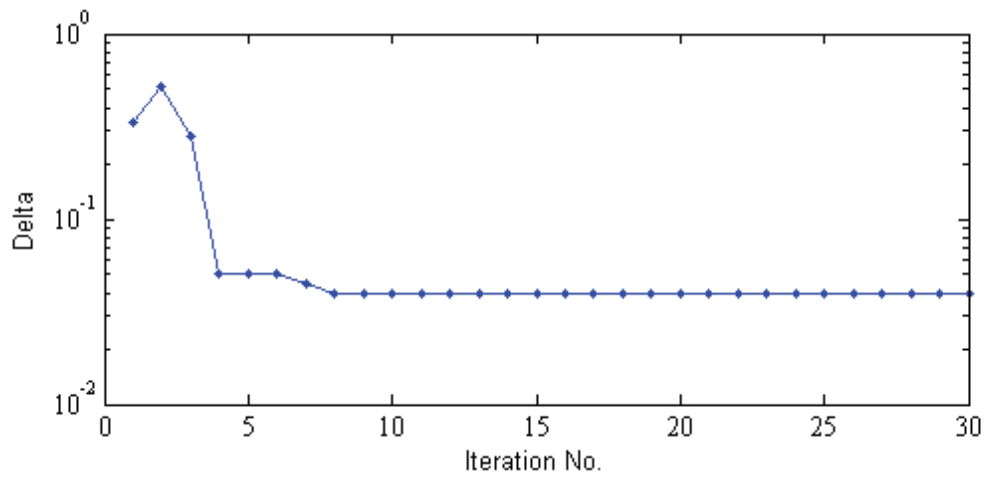
(a)

(b)

Figure 3.1 Progressions of APP iterations demonstrating the failure of the APP method in the solution of a 30-bus multi-period market-based OPF ($M = 2$, $T_R = 20$ minutes, $t_0 \rightarrow$ 8:00PM): (a) result of solving the OPF with ramp limits set to 1% of generator capacity per minute; (b) result of solving the OPF with ramp limits set to 2% of generator capacity per minute. Delta is defined as the infinite norm of X and λ's relative iteration-to-iteration changes and Θ in (1-36). No contingency is considered in this example.

$$Y^{k+1} = \arg\min_{d(Y)\in D} f_2(Y) + \sum_{i=1}^{NCI} \begin{cases} \dfrac{\beta^k}{2}(Y_{m_i} - Y_{m_i}^k)^2 + \gamma(Y_{m_i}^k - X_{m_i}^k)(Y_{m_i} - X_{m_i}^k) \\ \quad + \mu_{m_i}^k Y_{m_i}, \quad \text{if } \mu_{m_i}^k + \gamma^k(Y_{m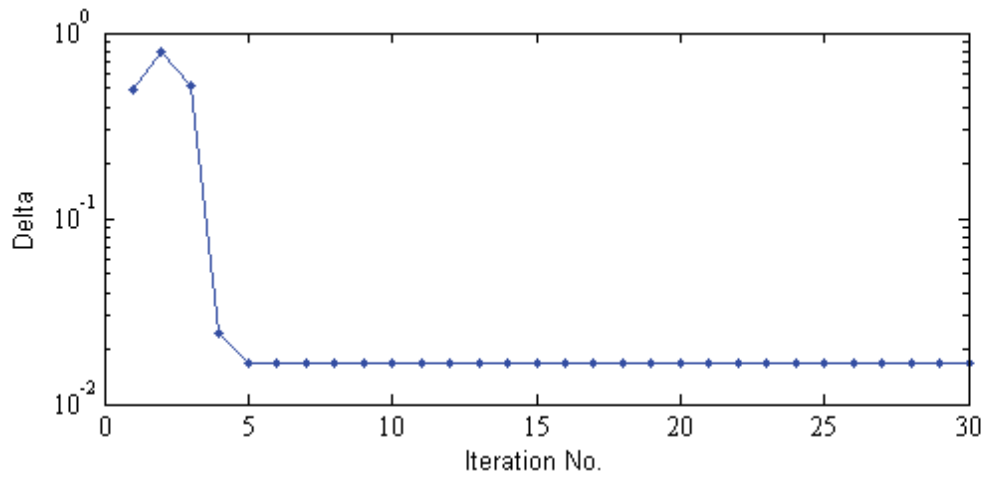_i}^k - X_{m_i}^k) > 0 \\ \\ 0, \quad\quad\quad\quad \text{if } \mu_{m_i}^k + \gamma^k(Y_{m_i}^k - X_{m_i}^k) \le 0 \end{cases}, \quad (3\text{-}3)$$

$$\mu_{m_i}^{k+1} = \max[0,\ \mu_{m_i}^k + \gamma^k(Y_{m_i}^{k+1} - X_{m_i}^{k+1})] \quad \text{for } i \in [1, NCI]$$

$$\bigcup_{i=1}^{NCI}\{X_{m_i}\} \equiv X_M; \quad \bigcup_{i=1}^{NCI}\{Y_{m_i}\} \equiv Y_M$$

$$\beta^{k+1} = \kappa\beta^k; \ \gamma^{k+1} = \kappa\gamma^k; \ \kappa > 1$$

where k is the iteration number. As in (1-36), convergence is achieved if X, Y, and μ's iteration-to-iteration changes are smaller than the tolerance and the inequality constraints among X and Y are satisfied. The handling of inequality constraints and the scaling of penalty parameters in (3-3) are similar to those of the augmented Lagrangian method discussed in Chapter 1 and Chapter 2. Figure 3.2 and 3.3 show the results of solving the same 30-bus multi-period OPF problem as in Table 3.1 and Figure 3.1 using the modified APP method.

Although the multi-period security-constrained OPF problem in (1-10) is now decomposable using the modified APP method, the large number of sequential iterations required, as shown in Figure 3.2, is still a significant computational hurdle for most real-time applications. For larger power systems, the modified APP method has difficulty of achieving consistent convergence.

3.2 Estimation and reduction of binding ramping constraints

In Chapter 1, it has been stated that the chief obstacle of decomposing the multi-period security-constrained OPF problem at the matrix computation level is the matrix fill-ins

Figure 3.2 Results of solving 72 consecutive 30-bus multi-period market-based OPF's using the modified APP method ($M = 2$, $T_R = 20$ minutes, $t_0 \rightarrow$ 8:00PM, $RA = 1\%$ of generator capacity per minute): (a) Iterations taken to solve the multi-period OPF's with $\kappa = 1.5$; (b) Iterations taken to solve the multi-period OPF's with $\kappa = 4$. No contingency is considered in this example.
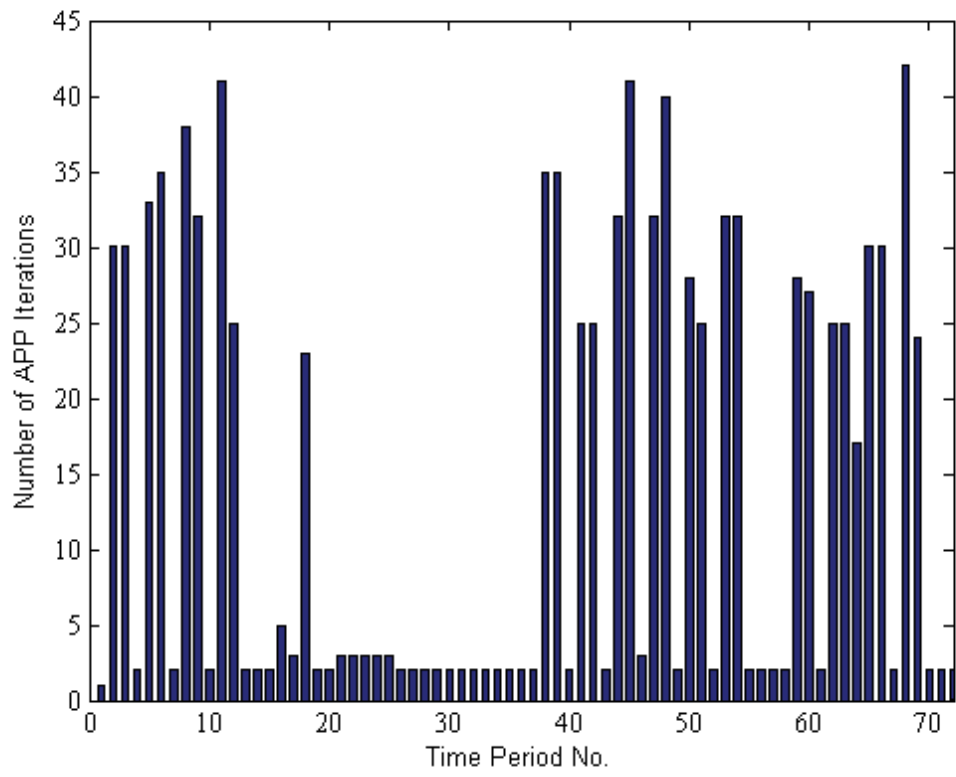
(a)

Figure 3.2 (Continued)
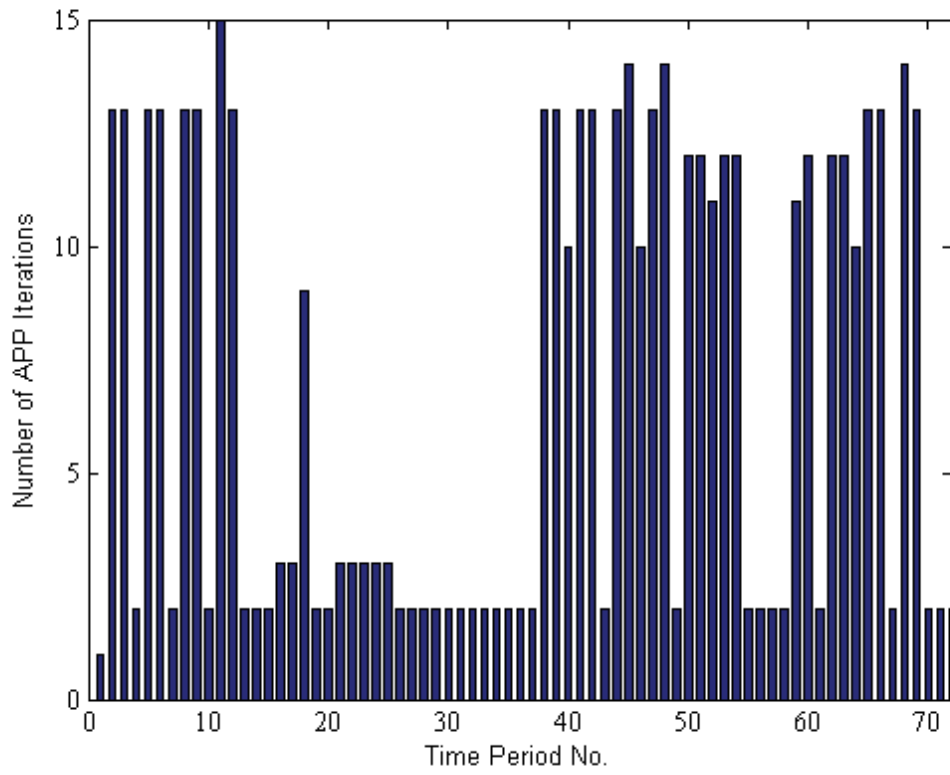
(b)
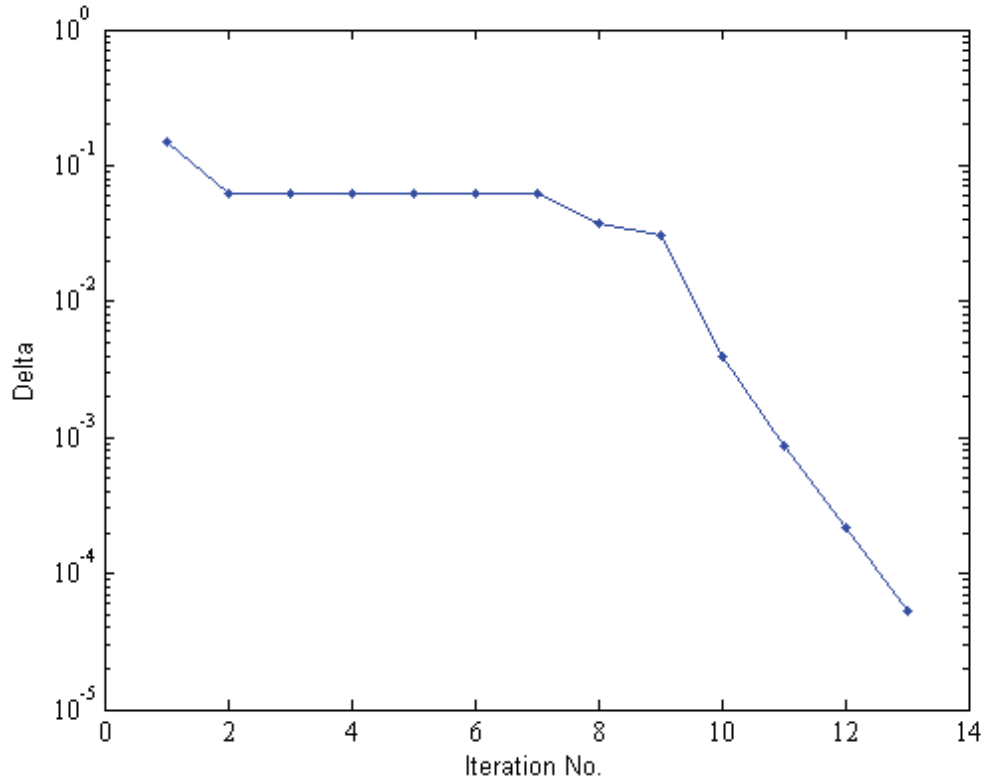
Figure 3.3 Progressions of APP iterations showing the success of the modified APP method in solving the 30-bus multi-period market-based OPF for the $t_0 + 1$ time period ($M = 2$, $T_R = 20$ minutes, $t_0 \rightarrow$ 8:00PM, $RA = 1\%$ of generator capacity per minute, $\kappa = 4$). Delta is defined as the infinite norm of X, Y and μ's relative iteration-to-iteration changes and $(Y - X)$ for binding $Y \leq X$ in (3-1) and (3-3). No contingency is considered in this example.

associated with the time-coupling and contingency-coupling generator ramping constraints. If the number of such coupling inequality constraints can be significantly reduced, one would be able to reorganize the Hessian matrix in (1-34) into the BDB form with much thinner boarder blocks, making it possible to decompose and parallelize the underlying matrix computation without much overhead.

While the number of generator ramping constraints in (1-10) is large, the number of binding ones can be small and manageable. The number of binding time-coupling constraints largely depends on the volatility of the market. Table 3.2 shows how this number changes with the volatility of the market, which is defined as the average period-to-period price fluctuation in percentage. The number of binding contingency-coupling constraints is determined by both the number of credible contingencies and the magnitudes of impacts that these credible contingencies have on the system. The number of credible contingencies identified by the contingency selection program is usually very small compared to the size of the system [5, 14, 33, 34]. The number of binding and treatable ones is even smaller, because most credible contingencies are either too severe to be treated in real-time dispatching operations, or too trivial to move the post-contingency dispatches close to the ramping limits. For example, an experiment of solving a 24-hour 30-bus comprehensive OPF shows that none of the 42 single-branch outage contingencies and the 6 single-generator outage contingencies is relevant: the single-generator outage contingencies are not treatable in real-time operations without commitment of new spinning reserve, the outage of No. 10 or No. 36 branch creates islands, and the rest single-branch outage contingencies are trivial.

Eliminating non-binding generator ramping constraints from (1-10) requires identification of which constraints are binding and which ones are not. Although an accurate identification is impossible without actually solving (1-10), one can gain a reasonably good estimate by solving a series of single-period OPF's for the future

Table 3.2 Number of generators that hit ramping limits in the solution of 30-bus multi-period market-based OPF's for 72 consecutive time periods. ($M = 3$, $T_R = 20$ minutes). Volatility is measured by the average period-to-period price fluctuation in percentage.

Market Volatility (%)	Max Number of Ramp-Limited Generators
0	1
10	2
20	2
30	2
40	4
50	4
60	5
70	5
80	5
90	6
100	6

periods in a look-ahead style, as outlined in Algorithm 3.1. In this method, a base-case single-period OPF is solved for each time period $t \in [t_0, t_0 + M]$ as

$$\min_{P_t, Q_t, V_t, \theta_t} \quad C_t(P_t, Q_t, V_t, \theta_t)$$

$$\text{s.t.} \quad FA_{i,t}(P_t, V_t, \theta_t) = 0$$

$$FR_{i,t}(Q_t, V_t, \theta_t) = 0$$

$$\max[P_{j,t0-1} - (t - t0 + 1)RA_j \Delta T_R, P_j^{\min}] - P_{j,t} \leq 0$$

$$P_{j,t} - \min[P_{j,t0-1} + (t - t0 + 1)RA_j \Delta T_R, P_j^{\max}] \leq 0$$

$$Q_j^{\min} \leq Q_{j,t} \leq Q_j^{\max}$$

$$V_i^{\min} \leq V_{i,t} \leq V_i^{\max}$$

$$|SF_k(V_t, \theta_t)| \leq S_k^{\text{nt-max}}$$

$$|ST_k(V_t, \theta_t)| \leq S_k^{\text{nt-max}}$$

$$i \in [1, NB], \quad j \in [1, NG], \quad k \in [1, NL] \qquad , \qquad (3\text{-}4)$$

where the ramping constraints between P_t and P_{t-1} in (1-10) are approximated by the constraints between P_t and P_{t0-1}. Since P_{t0-1} is readily available from the state estimator, the problem in (3-4) for each time period $t \in [t_0, t_0 + M]$ can be solved independently. Similarly, a single-period OPF is solved for each contingency case $t \in [t_0, t_0 + M], ci \in [1, NC]$ as

$$\min_{P_t^{ci}, Q_t^{ci}, V_t^{ci}, \theta_t^{ci}} \quad C_{zero}(P_t^{ci}, Q_t^{ci}, V_t^{ci}, \theta_t^{ci}) \equiv 0$$

$$FA_{i,t}^{ci}(P_t^{ci}, V_t^{ci}, \theta_t^{ci}) = 0$$

$$FR_{i,t}^{ci}(Q_t^{ci}, V_t^{ci}, \theta_t^{ci}) = 0 \qquad (3\text{-}5)$$

$$\max[P_{j,t0-1} - (t - t0 + 1)RA_j \Delta T_R, P_j^{\min}] - P_{j,t}^{ci} \leq 0$$

$$P_{j,t}^{ci} - \min[P_{j,t0-1} + (t - t0 + 1)RA_j \Delta T_R, P_j^{\max}] \leq 0$$

Algorithm 3.1

1. *Solve all individual single-period OPF's in (3-4) and (3-5) in parallel;*

2. *Estimate the binding ramping constraints based on the test in (3-6);*

3. *Formulate the comprehensive OPF in (3-7) with the estimated binding ramping constraints obtained from Step 2;*

4. *Solve (3-7) with TRALM, SC-PDIPM, or MCCV-PDIPM, with the underlying Hessian matrix reordered into the BDB form and relevant matrix computation decomposed and parallelized at the block level.*

$$Q_j^{\min} \le Q_{j,t}^{ci} \le Q_j^{\max}$$

$$\max(V_{i,t}^{ci-\min}, V_i^{\min}) \le V_{i,t}^{ci} \le \min(V_{i,t}^{ci-\max}, V_i^{\max})$$

$$|SF_k^{ci}(V_t^{ci}, \theta_t^{ci})| \le \min(S_{k,t}^{ci-\max}, S_k^{let-\max})$$

$$|ST_k^{ci}(V_t^{ci}, \theta_t^{ci})| \le \min(S_{k,t}^{ci-\max}, S_k^{let-\max}) \qquad . \qquad (3\text{-}5)$$

$$\Delta\theta_{i1,i2,t}^{ci-\min} \le \theta_{i1,t}^{ci} - \theta_{i2,t}^{ci} \le \Delta\theta_{i1,i2,t}^{ci-\max}$$

$$i \in [1, NB], \quad j \in [1, NG], \quad k \in [1, NL]$$

$$i1 \in [1, NB], \quad i2 \in [1, NB]$$

Once the above individual single-period OPF's have been solved, one can estimate the list of binding ramping constraints based on the following test:

if $P_{j,t}^* - P_j^{\min} \ge \varepsilon$ and $P_{j,t}^* - (P_{j,t-1}^* - RA_j\Delta T_R) \le \varepsilon$

$\quad (P_{j,t-1} - RA_j\Delta T_R) - P_{j,t} \le 0$ is considered binding

else

$\quad (P_{j,t-1} - RA_j\Delta T_R) - P_{j,t} \le 0$ is considered not binding

if $P_j^{\max} - P_{j,t}^* \ge \varepsilon$ and $(P_{j,t-1}^* + RA_j\Delta T_R) - P_{j,t}^* \le \varepsilon$

$\quad P_{j,t} - (P_{j,t-1} + RA_j\Delta T_R) \le 0$ is considered binding

else

$\quad P_{j,t} - (P_{j,t-1} + RA_j\Delta T_R) \le 0$ is considered not binding

if $P_{j,t}^{ci*} - P_j^{\min} \ge \varepsilon$ and $P_{j,t}^{ci*} - (P_{j,t}^* - RA_j\Delta T_R) \le \varepsilon$

$\quad (P_{j,t} - RA_j\Delta T_R) - P_{j,t}^{ci} \le 0$ is considered binding

else

$\quad (P_{j,t} - RA_j\Delta T_R) - P_{j,t}^{ci} \le 0$ is considered not binding

(3-6)

if $P_j^{\max} - P_{j,t}^{ci}{}^* \geq \varepsilon$ and $(P_{j,t}{}^* + RA_j \Delta T_R) - P_{j,t}^{ci}{}^* \leq \varepsilon$

$\quad P_{j,t}^{ci} - (P_{j,t} + RA_j \Delta T_R) \leq 0$ is considered binding

else $\hspace{9cm}$ (3-6)

$\quad P_{j,t}^{ci} - (P_{j,t} + RA_j \Delta T_R) \leq 0$ is considered not binding

$j \in [1, NG], \ t \in [t_0, t_0 + M], \ ci \in [1, NC]$

In (3-6), P^* is from the solutions of (3-4) and (3-5); neighboring dispatches are checked against each other to determine whether the ramping constraints between them are likely binding. The estimated set of binding ramping constraints is then used as a proxy for the actual binding set in the reformulation of (1-10), given by

$$\min_{P,Q,V,\theta} \ \sum_{t=t0}^{t0+M} C_t(P_t, Q_t, V_t, \theta_t)$$

s.t. $\quad P$ satisfies the estimated binding generator ramping constraints

$\quad FA_{i,t}(P_t, V_t, \theta_t) = 0$

$\quad FR_{i,t}(Q_t, V_t, \theta_t) = 0$

$\quad P_j^{\min} \leq P_{j,t} \leq P_j^{\max}$

$\quad Q_j^{\min} \leq Q_{j,t} \leq Q_j^{\max}$

$\quad V_i^{\min} \leq V_{i,t} \leq V_i^{\max}$

$\quad | SF_k(V_t, \theta_t) | \leq S_k^{\mathrm{nt-max}}$

$\quad | ST_k(V_t, \theta_t) | \leq S_k^{\mathrm{nt-max}}$

$\quad P_{j,t0-1} - RA_j \Delta T_R \leq P_{j,t0} \leq P_{j,t0-1} + RA_j \Delta T_R$

$\quad FA_{i,t}^{ci}(P_t^{ci}, V_t^{ci}, \theta_t^{ci}) = 0$

$\quad FR_{i,t}^{ci}(Q_t^{ci}, V_t^{ci}, \theta_t^{ci}) = 0 \hspace{4cm}$ (3-7)

$\quad P_j^{\min} \leq P_{j,t}^{ci} \leq P_j^{\max}$

$$Q_j^{\min} \le Q_{j,t}^{ci} \le Q_j^{\max}$$

$$\max(V_{i,t}^{ci-\min}, V_i^{\min}) \le V_{i,t}^{ci} \le \min(V_{i,t}^{ci-\max}, V_i^{\max})$$

$$|SF_k^{ci}(V_t^{ci}, \theta_t^{ci})| \le \min(S_{k,t}^{ci-\max}, S_k^{\text{let}-\max})$$

$$|ST_k^{ci}(V_t^{ci}, \theta_t^{ci})| \le \min(S_{k,t}^{ci-\max}, S_k^{\text{let}-\max}) \qquad\qquad . \qquad (3\text{-}7)$$

$$\Delta\theta_{i1,i2,t}^{ci-\min} \le \theta_{i1,t}^{ci} - \theta_{i2,t}^{ci} \le \Delta\theta_{i1,i2,t}^{ci-\max}$$

$$i \in [1, NB], \ \ j \in [1, NG], \ \ k \in [1, NL], \ \ i1 \in [1, NB], \ \ i2 \in [1, NB]$$

$$ci \in [1, NC], \ \ t \in [t_0, t_0 + M]$$

Now, one can solve (3-7) using TRALM, SC-PDIPM, or MCCV-PDIPM introduced in Chapter 2. Since the off-diagonal blocks of the Hessian matrix have been greatly shrunk as a result of the transformation in (3-7), one can reorder the Hessian matrix into the BDB form, and decompose and parallelize the NLP at the block matrix computation level with much less overhead. Table 3.3 compares the results of solving the original comprehensive OPF problem in (1-10) and the approximated comprehensive OPF problem in (3-7). The approximated comprehensive OPF offers a similar level of improvement over the single-period OPF as the original comprehensive OPF does.

As stated before, the number of binding contingency-coupling constraints is small and negligible. In a volatile market, however, the number of binding time-coupling constraints can become too large for one to adopt matrix-level decompositions, due to the overhead associated with matrix fill-ins. In such case, one can limit the list of estimated binding time-coupling constraints to a fixed size, and take only those constraints that are most critical to the optimization. Algorithm 3.2 integrates this procedure with Algorithm 3.1 to reduce the complexity of solving the comprehensive OPF. For comparisons, Algorithm 3.2 offers two ways of selecting the list of binding time-coupling constraints: one based on the magnitudes of ramping limits violations

Table 3.3 Comparisons of cumulative objective values of solving the 30-bus comprehensive multi-period security-constrained OPF's for 72 consecutive periods (T_R = 20 minutes) with and without the estimation and reduction (ER) of binding ramping constraints procedure in Algorithm 3.1.

Market Volatility (%)	$M = 0$	$M = 3$ without ER	$M = 3$ with ER
0	3.3634e5	3.3634e5	3.3634e5
10	3.1826e5	3.1818e5	3.1818e5
20	2.9987e5	2.9971e5	2.9971e5
30	2.8134e5	2.8099e5	2.8102e5
40	2.6250e5	2.6174e5	2.6175e5
50	2.4299e5	2.4194e5	2.4196e5
60	2.2326e5	2.2196e5	2.2200e5
70	2.0340e5	2.0147e5	2.0160e5
80	1.8363e5	1.8123e5	1.8138e5
90	1.6501e5	1.6302e5	1.6308e5
100	1.5043e5	1.4495e5	1.4602e5

Algorithm 3.2

1. *Solve all individual single-period OPF's in (3-4) and (3-5) in parallel;*

2. *Estimate the binding ramping constraints based on the test in (3-6);*

3. **If** *ER is set to VF*

   a. *Rank the estimated binding ramping constraints obtained from Step 2 according to their $| P_{j,t}{}^* - (P_{j,t-1}{}^* \pm RA_j \Delta T_R) |$ values;*

   else if *ER is set to CF*

   b. *Rank the estimated binding ramping constraints obtained from Step 2 according to their associated generator capacity $P_j^{\max}$ values;*

   end if

4. *Select MB highest ranked constraints from the list obtained in Step 3*

5. *Formulate the comprehensive OPF in (3-7) with the selected estimated binding ramping constraints obtained from Step 4;*

6. *Solve (3-7) with TRALM, SC-PDIPM, or MCCV-PDIPM, with the underlying Hessian matrix reordered into the BDB form and relevant matrix computation decomposed and parallelized at the block level.*

(*ER* is set to *VF*) and the other based on generator capacities (*ER* is set to *CF*). In the former, a fixed number (*MB*) of estimated binding time-coupling constraints acquired through (3-6) with largest $| P_{j,t}{}^{*} - (P_{j,t-1}{}^{*} \pm RA_{j}\Delta T_{R}) |$ values are retained in (3-7), while the rest are ignored. In the latter, *MB* estimated binding time-coupling constraints whose corresponding generators have largest capacities are selected. Table 3.4 shows the results of solving the 30-bus comprehensive multi-period security-constrained OPF's using Algorithm 3.2. It is evident that selecting binding constraints based on magnitudes of violations is better than selecting constraints based on generator capacities, as it yields results closer to the ideal ones (those computed without ER).

The number of estimated binding time-coupling constraints (*MB*) selected in Algorithm 3.2 affects both the optimality and the efficiency of the OPF computation. Table 3.5, 3.6, and 3.7 compare the results of solving (3-7) using Algorithm 3.2 with different *MB* values. The larger the *MB* is, the better the results match the ideal ones. Setting *MB* to ten percent of the total number of generators is often enough to generate satisfactory results. A large *MB*, however, may hurt the performance of the computation. In Algorithm 3.1 and 3.2, the bottleneck of the computation lies in Step 4 and Step 6, respectively, assuming standard block matrix computation techniques are used to handle the BDB Hessian matrix [61] and the load of the computation is coarsely and uniformly distributed among $(M+1)\times(NC+1)$ identical computational nodes. The nodal complexity of Algorithm 3.2 is similar to the complexity of solving a single-period base-case OPF using TRALM, SC-PDIPM, or MCCV-PDIPM, except that there is an additional cubic term on *MB* that is associated with the factorization of the dense boarder matrix block. Using TRALM, the nodal complexity of Algorithm 3.2 is

Table 3.4 Comparisons of cumulative objective values of solving the 30-bus comprehensive multi-period security-constrained OPF's for 72 consecutive periods (T_R = 20 minutes) with and without the estimation and reduction (ER) of binding ramping constraints procedure in Algorithm 3.2.

Market Volatility (%)	$M = 0$	$M = 3$ without ER	$M = 3$ with ER-VF, $MB = 2$	$M = 3$ with ER-CF, $MB = 2$
0	3.3634e5	3.3634e5	3.3634e5	3.3634e5
10	3.1826e5	3.1818e5	3.1818e5	3.1824e5
20	2.9987e5	2.9971e5	2.9971e5	2.9983e5
30	2.8134e5	2.8099e5	2.8102e5	2.8130e5
40	2.6250e5	2.6174e5	2.6189e5	2.6233e5
50	2.4299e5	2.4194e5	2.4207e5	2.4264e5
60	2.2326e5	2.2196e5	2.2225e5	2.2281e5
70	2.0340e5	2.0147e5	2.0198e5	2.0272e5
80	1.8363e5	1.8123e5	1.8169e5	1.8297e5
90	1.6501e5	1.6302e5	1.6323e5	1.6474e5
100	1.5043e5	1.4495e5	1.4610e5	1.4831e5

Table 3.5 Comparisons of cumulative objective values of solving the 30-bus comprehensive multi-period security-constrained OPF's for 72 consecutive periods (T_R = 20 minutes, Market Volatility = 100%) using Algorithm 3.2 (*ER* set to *VF)* with different *MB*'s

MB	$M = 3$ with ER-VF
0 ($M = 0$)	1.5043e5
1	1.4831e5
2	1.4610e5
3	1.4607e5
4	1.4606e5
5	1.4602e5
6 (without ER)	1.4495e5

Table 3.6 Comparisons of cumulative objective values of solving 118-bus comprehensive multi-period security-constrained OPF's for 72 consecutive periods (T_R = 20 minutes, Market Volatility = 100%) using Algorithm 3.2 (*ER* set to *VF)* with different *MB*'s

MB	$M = 3$ with ER-VF
0 ($M = 0$)	3.4328e6
5	3.3717e6
10	3.3376e6
15	3.3231e6
20	3.3044e6
25	3.2984e6
without ER	3.2885e6

Table 3.7 Comparisons of cumulative objective values of solving 2383-bus comprehensive multi-period security-constrained OPF's for 72 consecutive periods (T_R = 20 minutes, Market Volatility = 100%) using Algorithm 3.2 (*ER* set to *VF)* with different *MB*'s

MB	*M* = 3 with ER-VF
0 (*M* = 0)	3.1131e7
10	3.0905e7
20	3.0874e7
30	3.0861e7
40	3.0854e7
50	3.0854e7
without ER	3.0854e7

$$COMP_{COPF-ER-TRALM}(NB, NG, NL, NS, \alpha) = NI_{ALM} \times NI_{TRS} \times$$

$$NI_{TRM}(NB, NG, NL, NS, \alpha) \times \quad . \qquad (3\text{-}8)$$

$$[O(NB) + O(NL) + O(NG) + O(MB^3)]$$

Using SC-PDIPM, the nodal complexity is

$$COMP_{COPF-ER-SCPDIPM}(NB, NG, NL, NS, \alpha) =$$

$$NI_{SCPDIPM}(NB, NG, NL, NS, \alpha) \times \quad . \qquad (3\text{-}9)$$

$$[O(NB) + O(NL) + O(NG) + O(MB^3)]$$

And Using MCCV-PDIPM, the nodal complexity is

$$COMP_{COPF-ER-MCCV}(NB, NG, NL, NS) = NI_{MCCV}(NB, NG, NL, NS) \times$$

$$[O(NB) + O(NL) + O(NG) + O(NS) + O(MB^3)] \qquad (3\text{-}10)$$

Thus, a good choice of *MB* requires balancing the conflicting needs for both optimal OPF results and good computational performance. For systems with thousands of buses or more, the computational effort represented by the cubic terms on *MB* in (3-8), (3-9), and (3-10) is less than that represented by the linear terms, as long as *MB* is in the low hundreds or less.

Chapter 4

Conclusions

This work proposes, for the first time, the formulation and solution of a multi-period security-constrained OPF problem for real-time operations of electricity markets. The proposed OPF is intended to be part of the core pricing mechanism for electricity trading in open markets where real energy, reactive energy, voltages support, and other system resources and services are all traded in discrete bids and offers. Traditionally, real-time dispatching operations only involve single-period SCOPF's. This work demonstrates the need for comprehensive multi-period SCOPF's.

The nonsmoothness of offer/bid-driven OPF's is studied. Three techniques, namely, a trust-region based augmented Lagrangian method (TRALM), a step-controlled primal-dual interior point method (SC-PDIPM), and a modified constrained cost variables (MCCV) method, are developed for reliable and efficient computation of large-scale nonsmooth market-based OPF's. Numerical studies show that these techniques are reliable and better than some existing ones. MCCV (in conjunction with PDIPM) and SC-PDIPM are particularly good for real-time applications due to their efficiencies, while TRALM can be applied as a backup technique that offers global convergence guarantee. The CCV method has been extended to solve all Class-5 composite nonsmooth problems. Compared to the separable programming method DPOB, MCCV offers better scalability.

To reduce the computational complexity of solving the multi-period SCOPF problem, two decomposition techniques are proposed and studied. In the first one, the

APP decomposition method is extended to handle the inequality constraints that result from generator ramping limits. In the second one, binding time-coupling and contingency-coupling constraints are estimated, ranked, and filtered before the OPF computation is decomposed and parallelized using standard block matrix computation techniques. According to experimental results, the most promising way of solving large-scale multi-period SCOPF problems in real time is to combine the second decomposition method with the MCCV method.

The OPF formulation and relevant computation techniques proposed in this work balance the needs for: (1) deterministic convergence, (2) accurate computation of nodal prices, (3) support of both smooth and nonsmooth costings of a variety of resources and services, such as real energy, reactive energy, voltage support, etc., (4) full active and reactive power flow modeling of large-scale systems, and (5) satisfactory worst-case performance that meets the real-time dispatching requirement.

4.1 Limitations of this work

This work does not address the issue of global optimality. As mentioned in the discussion of MCCV, market-based OPF's containing non-convex costs demand complimentary global optimization techniques. Global optimization is, however, often a tedious computational task. It remains to be seen whether any recent development in the field of global optimization can bear fruits for real-time market-based OPF applications [62-64].

Infeasibility of the comprehensive multi-period SCOPF is another topic that is missing from this work. As pointed out earlier, most contingencies are either too trivial to influence OPF results or too severe to be remedied by available dispatchable reserves. In fact, it will most likely prove vain to consider contingencies at all in the

real-time OPF. To this end, the hourly balancing market might be a better place to address the issue of infeasibility and security constraints [36, 39]. Since generator units are free to be brought on-line or off-line in the balancing market, a balancing market evaluation (BME) requires the solution of a unit commitment problem. It will be worthwhile to study the integration of the real-time comprehensive OPF and the BME operations in the future.

Appendix A

System data

In this study, the 30-bus, 57-bus, 118-bus, and 300-bus system data are from the MATPOWER software package [57], and the 2383-bus and 2935-bus system data are proprietary and derived from real power systems.

To create random piecewise linear energy-cost data for a generator whose minimum real-power output is P_{min} and maximum real-power output is P_{max}, the range of real-power output is first divided into NS blocks:

$$[P_{min}, \ P_{min} + (P_{max} - P_{min})/NS\,),$$

$$[P_{min} + (P_{max} - P_{min})/NS, \ P_{min} + 2(P_{max} - P_{min})/NS\,),$$

$$[P_{min} + 2(P_{max} - P_{min})/NS, \ P_{min} + 3(P_{max} - P_{min})/NS\,),$$

$$\ldots$$

$$[P_{min} + (NS - 2)(P_{max} - P_{min})/NS, \ P_{min} + (NS - 1)(P_{max} - P_{min})/NS\,),$$

$$[P_{min} + (NS - 1)(P_{max} - P_{min})/NS, \ P_{max}].$$

The maximum energy offer price R_{max} is randomly generated in the range [\$50/MWh, \$100/MWh] with a uniform probability distribution. Then, for the ith block of real-power generation above, the energy offer price is set to $i \cdot R_{max}/NS$. The cost at the minimum-output point P_{min} is set to $P_{min} \cdot R_{max}/NS$.

To create random quadratic energy-cost data for a generator, two parameters, a and b, are randomly generated with uniform probability distributions in [\$50/MWh, \$100/MWh] and [\$0.0025/(MWh)^2, \$0.005/(MWh)^2], respectively. The energy cost is then expressed as $a \cdot P + 0.5\, b \cdot P^2$, where P is the real-power output of the generator.

Appendix B

Single-period OPF vs. multi-period

OPF in a 3-bus system example

The traditional single-period real-time OPF and the newly proposed multi-period real-time OPF are compared below using a 3-bus system example shown in Figure B.1. The MATPOWER-format [57] data of the 3-bus system is:

```
baseMVA = 100;
bus = [
 1  3   0   0  0  0  1  1  0  230  1  1.1  0.9;
 2  2  35  10  0  0  1  1  0  230  1  1.1  0.9;
 3  1  35  10  0  0  1  1  0  230  1  1.1  0.9;
];
gen = [
 1  0  0  50  -50  1  100  1  80  0;
 2  0  0  50  -50  1  100  1  60  0;
];
branch = [
 1  2  0.01  0.05  0.0  50  80  100  0  0  1;
 1  3  0.01  0.05  0.0  50  80  100  0  0  1;
 2  3  0.01  0.05  0.0  50  80  100  0  0  1;
];
areas = [
 1  1;
];
```

Loads and offer prices of 72 consecutive 20-minute periods (for one operating day) are listed in Table B.1, B.2, and B.3, and illustrated in Figure B.2 and B.3. In this
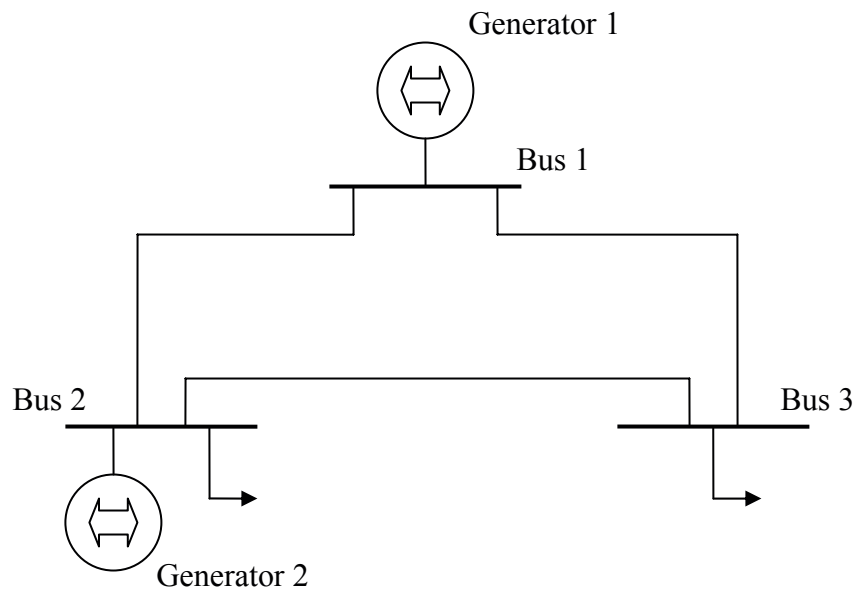
Figure B.1 System diagram of a 3-bus power system

Table B.1 72-period load levels (MW) at Bus 2/3 of the 3-bus power system (Bus 1's load is fixed at zero.)

Period	Load	Period	Load	Period	Load	Period	Load
1	35	19	33.394	37	38.211	55	43.028
2	35	20	33.394	38	38.211	56	43.028
3	35	21	33.394	39	38.211	57	43.028
4	33.716	22	34.679	40	37.89	58	43.349
5	33.716	23	34.679	41	37.89	59	43.349
6	33.716	24	34.679	42	37.89	60	43.349
7	33.073	25	36.284	43	37.248	61	42.385
8	33.073	26	36.284	44	37.248	62	42.385
9	33.073	27	36.284	45	37.248	63	42.385
10	32.752	28	37.89	46	36.606	64	41.101
11	32.752	29	37.89	47	36.606	65	41.101
12	32.752	30	37.89	48	36.606	66	41.101
13	32.11	31	38.532	49	36.927	67	39.174
14	32.11	32	38.532	50	36.927	68	39.174
15	32.11	33	38.532	51	36.927	69	39.174
16	32.431	34	38.532	52	38.853	70	36.606
17	32.431	35	38.532	53	38.853	71	36.606
18	32.431	36	38.532	54	38.853	72	36.606

Table B.2 72-period offer prices ($) for Generator 1 of the 3-bus power system

Period	Price	Period	Price	Period	Price	Period	Price
1	15.421	19	27.413	37	25.436	55	28.7
2	15.421	20	27.413	38	25.436	56	28.7
3	15.421	21	27.413	39	25.436	57	28.7
4	28.735	22	8.398	40	16.9	58	28.511
5	28.735	23	8.398	41	16.9	59	28.511
6	28.735	24	8.398	42	16.9	60	28.511
7	25.586	25	37.002	43	35.442	61	4.0555
8	25.586	26	37.002	44	35.442	62	4.0555
9	25.586	27	37.002	45	35.442	63	4.0555
10	4.4703	28	17.915	46	10.441	64	21.444
11	4.4703	29	17.915	47	10.441	65	21.444
12	4.4703	30	17.915	48	10.441	66	21.444
13	19.391	31	12.321	49	15.736	67	17.789
14	19.391	32	12.321	50	15.736	68	17.789
15	19.391	33	12.321	51	15.736	69	17.789
16	3.4034	34	7.9868	52	59.126	70	5.4889
17	3.4034	35	7.9868	53	59.126	71	5.4889
18	3.4034	36	7.9868	54	59.126	72	5.4889

Table B.3 72-period offer prices ($) for Generator 2 of the 3-bus power system

| Period	Price	Period	Price	Period	Price	Period	Price
1	6.5221	19	32.112	37	22.098	55	59.647
2	6.5221	20	32.112	38	22.098	56	59.647
3	6.5221	21	32.112	39	22.098	57	59.647
4	41.462	22	3.5328	40	31.847	58	8.634
5	41.462	23	3.5328	41	31.847	59	8.634
6	41.462	24	3.5328	42	31.847	60	8.634
7	51.431	25	7.9453	43	75.378	61	19.604
8	51.431	26	7.9453	44	75.378	62	19.604
9	51.431	27	7.9453	45	75.378	63	19.604
10	27.607	28	49.257	46	22.728	64	43.159
11	27.607	29	49.257	47	22.728	65	43.159
12	27.607	30	49.257	48	22.728	66	43.159
13	47.221	31	41.608	49	62.14	67	47.715
14	47.221	32	41.608	50	62.14	68	47.715
15	47.221	33	41.608	51	62.14	69	47.715
16	18.904	34	2.007	52	117.11	70	44.698
17	18.904	35	2.007	53	117.11	71	44.698
18	18.904	36	2.007	54	117.11	72	44.698
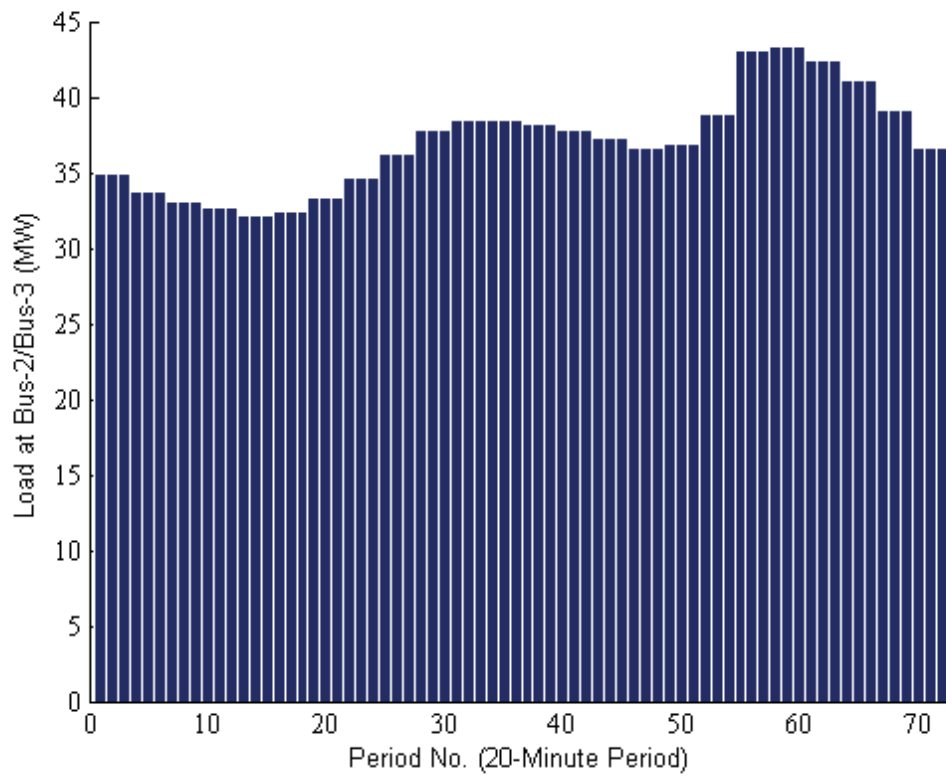
Figure B.2 Illustration of 72-period load changes at Bus 2/3 of the 3-bus power system
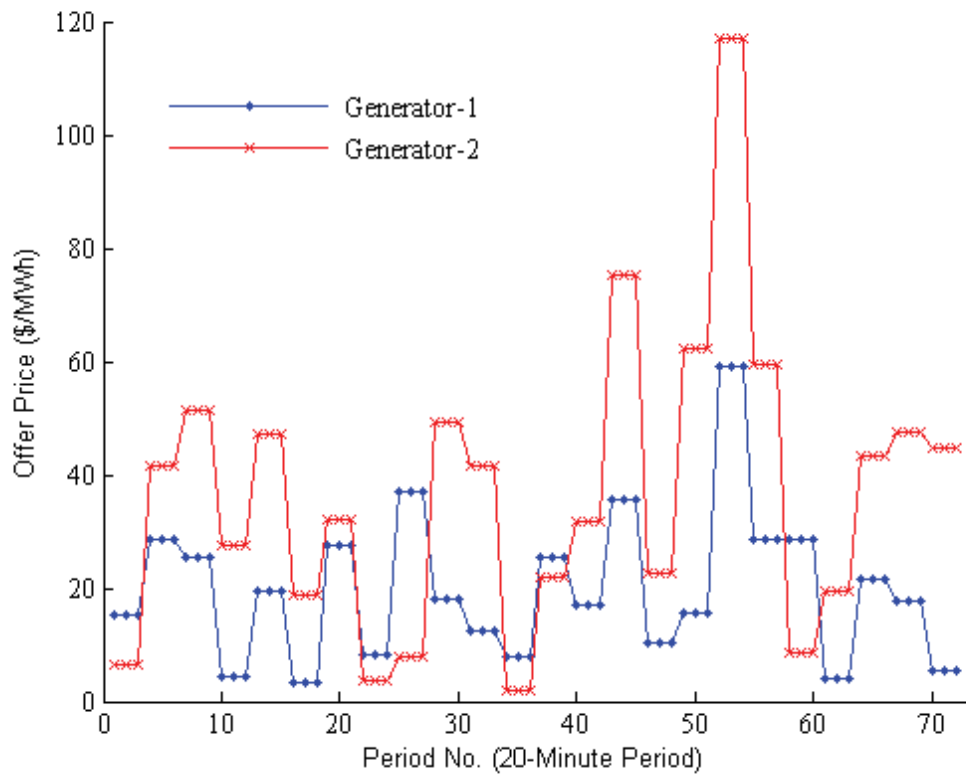
Figure B.3 Illustration of offer-price fluctuations in the 3-bus system example

experiment, reactive power is assumed to be constant and have no associated cost. Real-time dispatches are generated for the concerned 72 periods using single-period OPF's and multi-period OPF's; their associated operations costs, generator outputs, and LMPs are compared in Figure B.4, B.5, and B.6, which show that multi-period OPF's achieve approximately 4% daily cost savings over single-period OPF's, and yield noticeably different dispatches and LMPs.
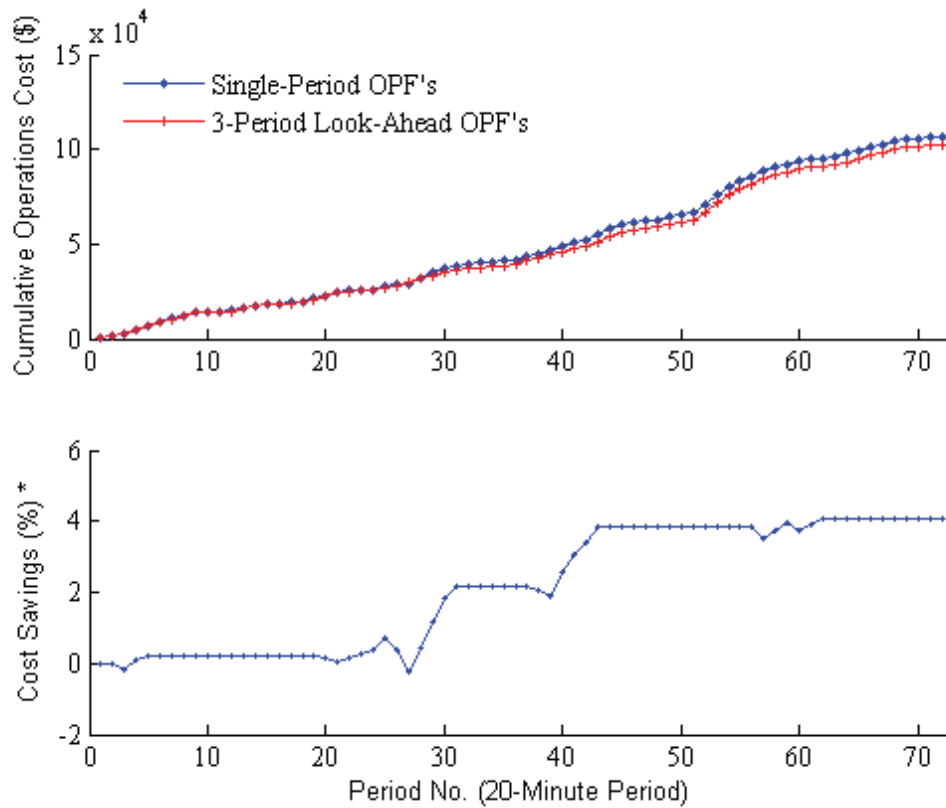
Figure B.4 Illustration of the growing difference between the cumulative cost of running real-time operations of the 3-bus power system using single-period OPF's and that of running the same operations using 3-period look-ahead OPF's. (* Percentage cost savings are defined as the multi-period OPF's cumulative dollar savings divided by the whole-day operations cost yielded by single-period OPF's.)
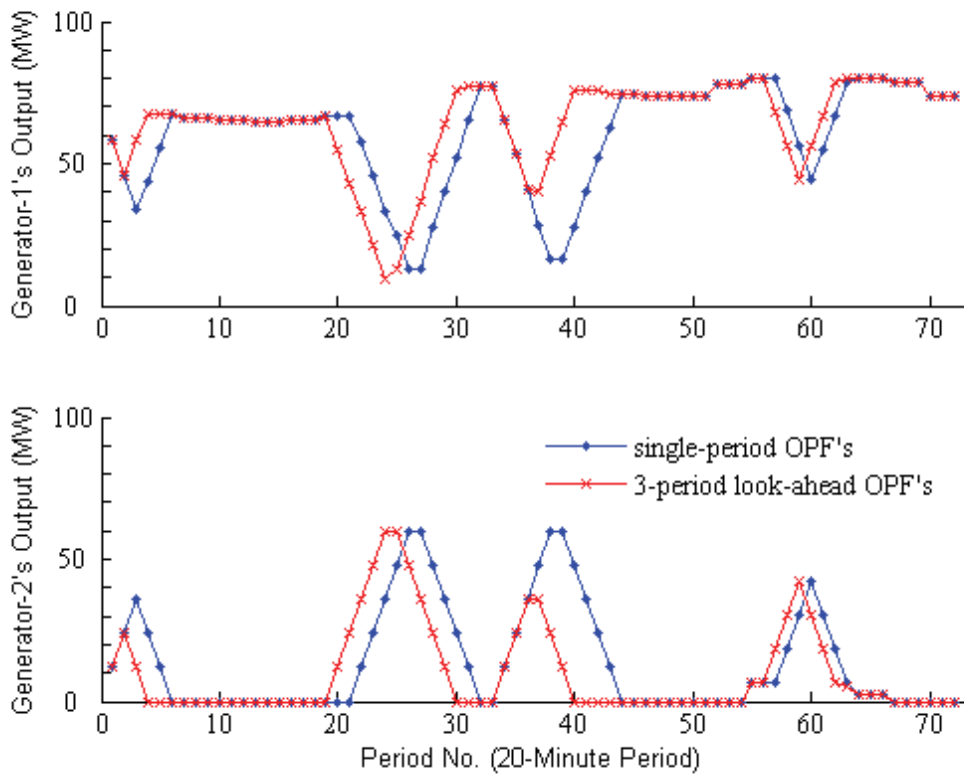
Figure B.5 Comparison of the generator outputs of the 3-bus power system dispatched by single-period OPF's and those by 3-period look-ahead OPF's.
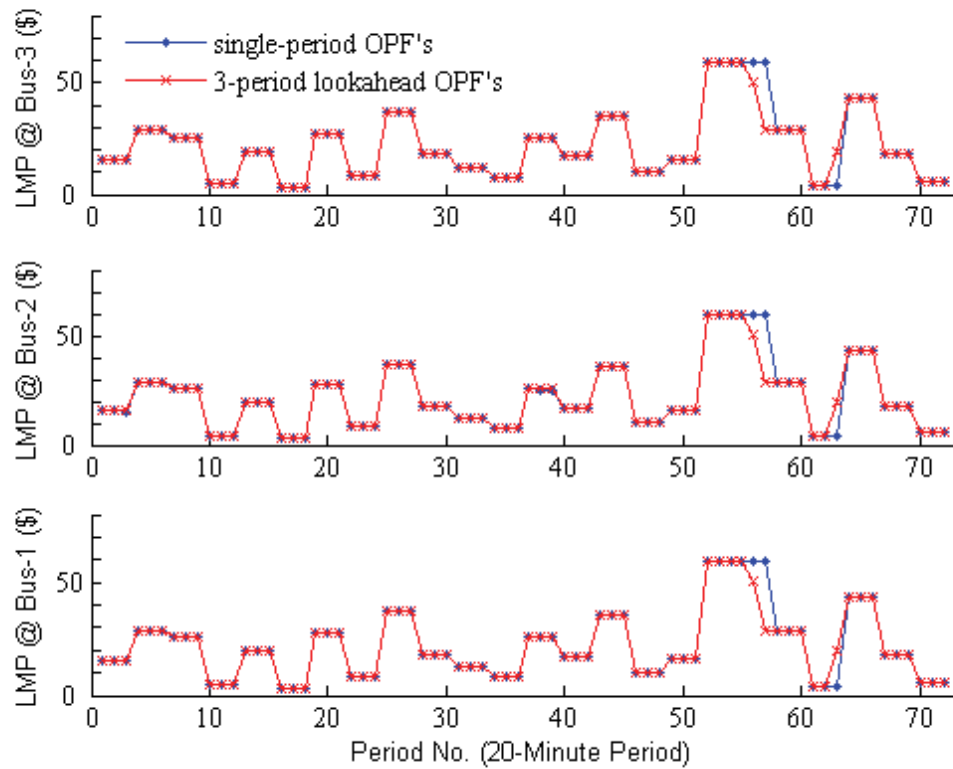
Figure B.6 Comparison of the LMPs of the 3-bus power system generated by single-period OPF's and those by 3-period look-ahead OPF's.

Bibliography

[1]   J. Carpentier, "Contribution a l'Etude du Dispatching Economique," Bulletin de la Societe Francaise des Electriciens, vol. 3, pp. 431–447, August 1962

[2]   O. Alsac and B. Stott, "Optimal Load Flow with Steady-State Security," IEEE Transactions on Power Apparatus and Systems, vol. PAS-93, no. 3, pp. 745-751, May 1974

[3]   B. Stott, O. Alsac, and A. J. Monticelli, "Security Analysis and Optimization,", Proceedings of the IEEE, vol. 75, no. 12, pp. 1623-1644, December 1987

[4]   O. Alsac, J. Bright, M. Prais, and B. Stott, "Further Developments in LP-Based Optimal Power Flow," IEEE Transactions on Power Systems, vol. 5, no. 3, pp. 697-711, August 1990

[5]   J. Carpentier and P. Bornard, "Towards an Integrated Secure Optimal Operation of Power Systems," Proceedings of the IEE International Conference on Advances in Power System Control, Operation and Management, November 1991

[6]   M. Huneault and F. D. Galiana, "A Survey of the Optimal Power Flow Literature," IEEE Transactions on Power Systems, vol. 6, no. 2, pp. 762-770, May 1991

[7]   S. Granville, "Optimal Reactive Dispatch through Interior Point Methods," IEEE Transactions on Power Systems, vol. 9, no. 1, pp. 136-146, February 1994

[8]   Y. Wu, A. S. Debs, and R. E. Marsten, "A Direct Nonlinear Predictor-Corrector Primal-Dual Interior Point Algorithm for Optimal Power Flows," IEEE Transactions on Power Systems, vol. 9, no. 2, pp. 876-883, May 1994

[9]   G. L. Torres and V. H. Quintana, "Optimal Power Flow by a Nonlinear Complementarity Method," IEEE Transactions on Power Systems, vol. 15, no. 3, pp. 1028-1033, August 2000

[10]   G. L. Torres and V. H. Quintana, "On a Nonlinear Multiple-Centrality-Corrections Interior-Point Method for Optimal Power Flow," IEEE Transactions on Power Systems, vol. 16, no.2, pp. 222-228, May 2001

[11]   E. D. Castronuovo, J. M. Campagnolo, R. Salgado, "On the Application of High Performance Computation Techniques to Nonlinear Interior Point Methods," IEEE Transactions on Power Systems, vol. 16, no. 3, pp. 325-331, August 2001

[12] R. A. Jabr, A. H. Coonick, B. J. Cory, "A Primal-Dual Interior Point Method for Optimal Power Flow Dispatching," IEEE Transactions on Power Systems, vol. 17, no. 3, pp. 654-662, August 2002

[13] W. Qiu, A. J. Flueck, and F. Tu, "A New Parallel Algorithm for Security Constrained Optimal Power Flow with a Nonlinear Interior Point Method," Proceedings of the Power Engineering Society General Meeting, 2005

[14] A. Monticelli, M. V. F. Pereira, and S. Granville, "Security-Constrained Optimal Power Flow with Post-Contingency Corrective Rescheduling," IEEE Transactions on Power Systems, vol. PWRS-2, no. 1, pp. 175-182, February 1987

[15] L. D. B. Terra and M. J. Short, "Security-Constrained Reactive Power Dispatch," IEEE Transactions on Power Systems, vol. 6, no. 1, pp. 109-117, February 1991

[16] M. Rodrigues, O. R. Saavedra, A. Monticelli, "Asynchronous Programming Model for the Concurrent Solution of the Security Constrained Optimal Power Flow Problem," IEEE Transactions on Power Systems, vol. 9, no. 4, pp. 2021-2027, November 1994

[17] V. C. Ramesh and S. N. Talukdar, "A Parallel Asynchronous Decomposition for On-Line Contingency Planning," IEEE Transactions on Power Systems, vol. 11, no. 1, pp. 344-349, February 1996

[18] C. E. Murillo-Sánchez and R. J. Thomas, "Thermal Unit Commitment Including Optimal AC Power Flow Constraints," Proceedings of the 30th Hawaii International Conference on System Sciences, 1997

[19] B. H. Kim and R. Baldick, "Coarse-Grained Distributed Optimal Power Flow," IEEE Transactions on Power Systems, vol. 12, no. 2, pp. 932-939, May 1997

[20] H. Harsan, N. Hadjsaid, P. Pruvot, "Cyclic Security Analysis for Security Constrained Optimal Power Flow," IEEE Transactions on Power Systems, vol. 12, no. 2, pp. 948-953, May 1997

[21] H. Ma and S. M. Shahidehpour, "Unit Commitment with Transmission Security and Voltage Constraints," IEEE Transactions on Power Systems, vol. 14, no. 2, pp. 757-764, May 1999

[22] C. E. Murillo-Sánchez, "On the Integration of Unit Commitment and Optimal Power Flow," Ph.D. Dissertation, Cornell University, January 2000

[23] N. Alguacil and A. J. Conejo, "Multiperiod Optimal Power Flow Using Benders Decomposition," IEEE Transactions on Power Systems, vol. 15, no. 1, pp. 196-201, February 2000

[24] B. H. Kim and R. Baldick, "A Comparison of Distributed Optimal Power Flow Algorithms," IEEE Transactions on Power Systems, vol. 15, no. 2, pp. 599-604, May 2000

[25] J. Carpentier, D. Menniti, N. Scordino, and N. Sorrentino, "An Algorithm for a Direct Solution of Active Secure Economic Dispatch with an Improved Economic Statement," Proceedings of the International Conference on Power System Technology, vol. 3, pp. 1239-1244, December 2000

[26] C. Beltran and F. J. Heredia, "Unit Commitment by Augmented Lagrangian Relaxation: Testing Two Decomposition Approaches," Journal of Optimization Theory and Applications, vol. 112, no. 2, pp. 295-314, February 2002

[27] A. Losi and M. Russo, "On the Application of the Auxiliary Problem Principle," Journal of Optimization Theory and Applications, vol. 117, no. 2, pp. 377-396, May 2003

[28] F. J. Nogales, F. J. Prieto, and A. J. Conejo, "A Decomposition Methodology Applied to the Multi-Area Optimal Power Flow Problem," Annals of Operations Research, vol. 120, pp. 99-116, 2003

[29] J. Chen, J. S. Thorp, and T. D. Mount, "Coordinated Interchange Scheduling and Opportunity Cost Payment: A Market Proposal of Seams Issues," Proceedings of the 37th Hawaii International Conference on System Sciences, 2004

[30] J. Chen, "Towards an Integrated and Seamless Market of Energy and Ancillary Services," Ph.D. Dissertation, Cornell University, May 2004

[31] H. Yamin, S. Al-Agtash, and M. Shahidehpour, "Security-Constrained Optimal Generation Scheduling for GENCOs," IEEE Transactions on Power Systems, vol. 9, no. 3, pp. 1365-1372, August 2004

[32] O. E. Moya, "A Spinning Reserve, Load Scheduling, and Economic Dispatch Solution by Bender's Decomposition," IEEE Transactions on Power Systems, vol. 20, no. 1, pp. 384-388, February 2005

[33] M. Shahidehpour, W. F. Tinney, and Y. Fu, "Impact of Security on Power Systems Operation," Proceedings of the IEEE, vol. 93, no. 11, pp. 2013-2025, November 2005

[34] J. Martínez-Crespo, Julio Usaola, and J. L. Fernández, "Security-Constrained Optimal Generation Scheduling in Large-Scale Power Systems," IEEE Transactions on Power Systems, vol. 21, no. 1, pp. 321-332, February 2006

[35] R. Bacher and H. P. V. Meeteren, "Real-Time Optimal Power Flow in Automatic Generation Control," IEEE Transactions on Power Systems, vol. 3, no. 4, pp. 1518-1529, November 1988

[36] New York Independent System Operator, NYISO Transmission and Dispatching Operations Manual, available at http://www.nyiso.com, September 1999

[37] New York Independent System Operator, NYISO Day-Ahead Scheduling Manual, available at http://www.nyiso.com, June 2001

[38] PJM Interconnection, PJM Manual 11: Scheduling Operations, rev. 29, available at http://www.pjm.com, August 2006

[39] PJM Interconnection, PJM Manual 12: Dispatching Operations, rev. 13, available at http://www.pjm.com, May 2006

[40] Federal Energy Regulatory Commission, "Principles for Efficient and Reliable Reactive Power Supply and Consumption", FERC Staff Reports, Docket No. AD05-1-000, pp. 161-162, available at http://www.ferc.gov/legal/staff-reports.asp, February 2005

[41] G. Cohen, "Auxiliary Problem Principle and Decomposition of Optimization Problems," Journal of Optimization Theory and Applications, vol. 32, no. 3, pp. 277-305, November 1980

[42] ABS Energy Research, "Electricity Deregulation Report: Global 2006", 5th edition, available at http://www.absenergyresearch.com, 2006

[43] S. Repo, "On-Line Voltage Stability Assessment of Power System – An Approach of Black-Box Modeling," Tampere University of Technology Publications 344, available at http://butler.cc.tut.fi/~repo/Julkaisut/SR_thesis.pdf, 2001

[44] M. Pavella, D. Ernst, and D. Ruiz-Vera, Stability of Power Systems: A Unified Approach to Assessment and Control, Springer, 2000

[45] D. P. Bertsekas, Nonlinear Programming, 2nd edition, Athena Scientific, 1999, pp. 397-426

[46] D. Gay, "Computing Optimal Locally Constrained Steps," SIAM Journal on Scientific and Statistical Computing, vol. 2, pp. 186-197, June 1981

[47] J. J. More and D. C. Sorensen, "Computing a Trust Region Step," SIAM Journal on Scientific and Statistical Computing, vol. 4, pp. 553-572, September 1983

[48] T. F. Coleman and Y. Li, "An Interior Trust Region Approach for Nonlinear Minimization Subject to Bounds," SIAM Journal on Optimization, vol. 6, pp. 418-445, May 1996

[49] M. A. Branch, T. F. Coleman, and Y. Li, "A Subspace, Interior, and Conjugate Gradient Method for Large-Scale Bound-Constrained Minimization Problems," SIAM Journal on Scientific Computing, vol. 21, pp. 1-23, August 1999

[50] D. P. Bertsekas, Nonlinear Programming, 2nd edition, Athena Scientific, 1999, pp. 95-97

[51] A. S. El-Bakry, R. A. Tapia, T. Tsuchiya, and Y. Zhang, "On the Formulation and Theory of the Newton Interior-Point Method for Nonlinear Programming," Journal of Optimization Theory and Applications, vol. 89, no. 3, pp. 507-541, June 1996

[52] D. P. Bertsekas, Nonlinear Programming, 2nd edition, Athena Scientific, 1999, pp. 455-481

[53] F. H. Clarke, Optimization and Nonsmooth Analysis, SIAM, 1990

[54] R. S. Womersley and R. Fletcher, "An Algorithm for Composite Nonsmooth Optimization Problems," Journal of Optimization Theory and Applications, vol. 48, no. 3, pp. 493-523, March 1986

[55] M. S. Bazaraa and C. M. Shetty, Nonlinear Programming – Theory and Algorithms, John Wiley & Sons, 1979, pp. 453-471

[56] R. Fletcher, Practical Methods of Optimization, 2nd edition, John Wiley & Sons, 1987, pp. 357-416

[57] R. D. Zimmerman, C. E. Murillo-Sánchez, and D. Gan, MATPOWER User's Manual, ver. 3.1b2, available at http://www.pserc.cornell.edu/matpower, September 2006

[58] A. M. Geoffrion, "Generalized Benders Decomposition," Journal of Optimization Theory and Applications, vol. 10, no. 4, pp. 237-260, 1972

[59] T. Davis, UFSparse, available at http://www.cise.ufl.edu/research/sparse

[60] B. D. Murtagh and M. A. Saunders, MINOS 5.5 User's Guide, Stanford University Systems Optimization Laboratory Technical Report SOL83-20R

[61] G. H. Golub and C. F. Van Loan, Matrix Computations, 3rd edition, The John Hopkins University Press, 1996

[62] L. Chambers, The Practical Handbook of Genetic Algorithms, Applications, 2nd edition, Chapman & Hall/CRC, 2001

[63] R. Horst, P. M. Pardalos, and N. V. Thoai, Introduction to Global Optimization, 2nd edition, Kluwer Academic Publishers, 2000

[64] M. Tawarmalani and N. V. Sahinidis, Convexification and Global Optimization in Continuous and Mix-Integer Nonlinear Programming: Theory, Algorithms, Software, and Applications, Kluwer Academic Publishers, 2002